

Expansion and intensification of the North American Monsoon during the Pliocene

Tripti Bhattacharya,^{1*} Ran Feng,² Jessica Tierney,³
Natalie Burls,⁴ Scott Knapp,⁴ Minmin Fu⁵

¹Department of Earth and Environmental Sciences, Syracuse University, Syracuse NY

²Department of Geosciences, University of Connecticut, Storrs CT

³Department of Geosciences, University of Arizona, Tucson AZ

⁴Department of Atmospheric, Oceanic and Earth Sciences, George Mason University, Fairfax VA

⁵Department of Earth and Planetary Sciences, Harvard University, Cambridge, MA

*To whom correspondence should be addressed; E-mail: trbhata@syr.edu.

This paper is a non-peer reviewed preprint submitted to EarthArXiv. It will be updated as the manuscript progresses through peer review.

1 **Expansion and intensification of the North American Monsoon** 2 **during the Pliocene**

3 **Tripti Bhattacharya**¹, **Ran Feng**², **Jessica E. Tierney**³, **Claire Rubbelke**¹, **Natalie Burls**⁴,
4 **Scott Knapp**⁴, **Minmin Fu**⁵

5 ¹Department of Earth and Environmental Sciences, Syracuse University, Syracuse NY

6 ²Department of Geosciences, University of Connecticut, Storrs CT

7 ³Department of Geosciences, University of Arizona, Tucson AZ

8 ⁴Department of Atmospheric, Oceanic and Earth Sciences, George Mason University, Fairfax VA

9 ⁵Department of Earth and Planetary Sciences, Harvard University, Cambridge, MA

10 **Key Points:**

- 11 • Leaf wax hydrogen isotopes preserved in ocean sediments reveal evidence of a stronger
12 mid-Pliocene monsoon in southwestern North America
- 13 • Isotope-enabled simulations show that a stronger monsoon resulted from a diminished
14 east Pacific subtropical-tropical temperature gradient
- 15 • This mechanism is relevant to understanding present-day monsoon variability in response
16 to California margin marine heat waves

Abstract

Southwestern North America, like many subtropical regions, is predicted to become drier in response to anthropogenic warming. However, during the Pliocene, when carbon dioxide was above pre-industrial levels, multiple lines of evidence suggest that southwestern North America was much wetter. While existing explanations for a wet Pliocene invoke increases in winter rain, recent modeling studies hypothesize that summer rain may have also played an important role. Here, we present the first direct evidence for an intensified mid-Pliocene monsoon in southwestern North America using leaf wax hydrogen isotopes. These new records provide evidence that the mid-Pliocene featured an intensified and expanded North American Monsoon. Using proxies and isotope-enabled model simulations, we show that monsoon intensification is linked to amplified warming on the southern California margin relative to the tropical Pacific. This mechanism has clear relevance for understanding present-day monsoon variations, since we show that intervals of amplified subtropical warming on the California margin, as are seen during modern California margin heat waves, are associated with a stronger monsoon. Because marine heat waves are predicted to increase in frequency, the future may bring intervals of ‘Pliocene-like’ rainfall that co-exist with intensifying megadrought in southwestern North America, with implications for ecosystems, human infrastructure, and water resources.

Plain Language Summary

The middle Pliocene, an interval approximately 3 million years ago, has long puzzled climate scientists. Despite having higher-than-preindustrial carbon dioxide levels, which should result in drier conditions in subtropical regions, some subtropical regions were wet during the Pliocene. In southwestern North America, there were large permanent lakes and plant and animal species that cannot exist in arid regions. We used measurements of hydrogen isotopes in ancient plant matter to show that wet conditions in the Pliocene southwest resulted from a stronger monsoon. This stronger monsoon was caused by changes in subtropical and tropical ocean temperatures in the eastern Pacific. This study presents the first direct evidence that monsoon changes caused wet conditions in the middle Pliocene. It also has relevance for the present, since we find evidence that present-day changes in subtropical ocean temperatures can amplify the monsoon, via a mechanism that strongly resembles what happened in the Pliocene. Our study suggests that further studies of the Pliocene can shed light on how future monsoon changes may influence wildfire, landscapes, and water resources across the southwest.

49 Introduction

50 Multiple lines of evidence suggest that southwestern North America (SWNA), like many
 51 subtropical continents, was much wetter during the Pliocene epoch, a climate interval featur-
 52 ing reduced ice volume and CO₂ concentrations above preindustrial levels (Figure 1). Sedi-
 53 mentological data document widespread perennial and ephemeral lakes in southern Califor-
 54 nia and Arizona (M. Pound et al., 2014; Ibarra et al., 2018) (Figure 1), and palynological and
 55 macrobotanical evidence from southern California suggests expanded tree cover and the pres-
 56 ence of species that today only grow in regions with mesic conditions and summer rainfall (Remeika
 57 et al., 1988; Ballog & Malloy, 1981). Faunal remains from Baja California contain *Crocody-*
 58 *lus* spp. fossils, which require freshwater habitats, further suggesting increased water resources
 59 in regions that are arid at present (Salzmann et al., 2009; Miller, 1980). At face value, this ev-
 60 idence for a wet Pliocene is at odds with the theoretical and model-derived prediction that re-
 61 gions like SWNA, and subtropical continents more broadly, will continue to dry in coming cen-
 62 turies as a result of elevated greenhouse gases (Byrne & O’Gorman, 2015; Seager et al., 2010).

63 Two dominant hypotheses have been proposed to explain the evidence for wet condi-
 64 tions in SWNA during the Pliocene. On a global scale, a dramatically weaker meridional sea
 65 surface temperature (SST) gradient could have weakened mean atmospheric circulation and
 66 reduced subtropical moisture divergence (Burls & Fedorov, 2017; A. V. Fedorov et al., 2015).
 67 However, current proxy-based estimates of SST patterns suggest that reductions in Pliocene
 68 meridional gradients were modest (Tierney et al., 2019). Another possibility is that a weaker
 69 Pacific Walker circulation shifted winter storm tracks southward, bringing increased moisture
 70 to SWNA, similar to what occurs during El Niño events today (Ibarra et al., 2018; Molnar &
 71 Cane, 2002). However, this hypothesis would require almost two-fold increases in winter rain-
 72 fall to explain Pliocene lake distributions, and cannot explain the presence of tree species like
 73 *Castanea* and *Carya* or the expansion of Sonoran desert flora, which are interpreted as indi-
 74 cators of summer rainfall (Ibarra et al., 2018; Ballog & Malloy, 1981; Axelrod, 1948). These
 75 qualitative data suggest a role for the North American Monsoon (NAM), which is the primary
 76 source of summer rainfall in the SWNA and maintains the floristically diverse ecosystems of
 77 the Sonoran Desert (Cook & Seager, 2013). Today, the NAM is restricted to southern Arizona,
 78 New Mexico and northwestern Mexico along the eastern side of the Gulf of California.

79 A recent modeling study found that warm coastal temperatures on the California mar-
 80 gin, similar to those observed in Pliocene proxy records, results in an expansion of summer
 81 rainfall across SWNA (Fu et al., 2022). In these simulations, precipitation rates associated with
 82 a stronger monsoon exceed evaporation. If these changes are realistic, they suggest that mon-
 83 soon changes alone could explain the mesic vegetation and high lake levels found in the Pliocene.
 84 However, the hypothesis that the NAM was stronger during the Pliocene, an interval charac-

85 terized by higher greenhouse gas forcing, is at odds with some model predictions of how the
86 NAM responds to higher atmospheric greenhouse gases (Pascale et al., 2017).

87 Current-generation models do not show consensus about the response of the NAM to
88 21st century warming, possibly as a result of systematic biases and low resolution that pre-
89 vents many models from accurately capturing California Margin and Gulf of California SSTs
90 (Maloney et al., 2014; Meyer & Jin, 2017; Cook & Seager, 2013; Almazroui et al., 2021; Moon
91 & Ha, 2020). A recent high-resolution modeling study with a bias-corrected SST field sug-
92 gests that the NAM will weaken in response to 21st century warming. In this simulation, the
93 NAM strength responds to the *relative* warming of SST in the subtropical eastern Pacific (e.g.
94 southern California Margin) (Pascale et al., 2017). Specifically, because the southern Califor-
95 nia margin warms at a slower rate than the tropical eastern equatorial Pacific (EEP), SWNA
96 experiences stronger descending motion and greater atmospheric stability, reducing NAM con-
97 vection. This strong sensitivity to SST gradients distinguishes the NAM from other monsoons,
98 which respond more strongly to direct CO₂ forcing. This conceptual model, similar to the ‘warmer-
99 get-wetter’ paradigm (Xie et al., 2010), suggests that past and future NAM strength depends
100 less on the *absolute* magnitude of warming on the southern California Margin, as suggested
101 by (Fu et al., 2022), but instead depends on the *gradient* of temperature between the subtrop-
102 ical eastern Pacific and the tropical eastern Pacific. This latter conceptual model has been ap-
103 plied to understanding NAM variations over the Holocene (Barron et al., 2012).

104 In light of this uncertainty, continuous Plio-Pleistocene, summer rainfall-sensitive proxy
105 records are invaluable for identifying the mechanisms that control long-term changes in NAM
106 rainfall. However, much of the existing proxy evidence from the Pliocene consists of non-continuous
107 snapshots of Pliocene climate, or proxies that can only be interpreted in a purely qualitative
108 framework. Here, we remedy this by presenting the first continuous Plio-Pleistocene records
109 of NAM region hydroclimate, based on leaf wax biomarkers in two marine sediment cores.
110 We focus on reconstructing hydroclimate between the mid-Pliocene, beginning at approximately
111 3.5 Ma, through the late Pleistocene, although the processes we explore may apply to the broader
112 Pliocene epoch. DSDP 475 is located near the tip of southern Baja California, immediately
113 west of the core modern NAM domain. Our second site, ODP 1012 is on the CA margin, north-
114 west of the NAM domain in the present climatology, and receives virtually no monsoon rain-
115 fall today. Together, these sites are especially sensitive to hydroclimate changes in the core
116 monsoon domain (DSDP 475), as well as any potential expansion of the monsoon into periph-
117 eral zones (ODP 1012). Previous work has shown that the hydrogen isotopic signature of ter-
118 restrial plant epicuticular waxes (δD_{wax}) reflects the δD signature of precipitation (δD_p) across
119 a range of ecosystem types (Sachse et al., 2012), and in SWNA, leaf wax δD is strongly sen-
120 sitive to the relative contribution of monsoonal deep convection to annual rainfall totals (Bhattacharya

121 et al., 2018). This proxy is therefore well-suited for investigating whether summer rainfall played
 122 a role in driving Plio-Pleistocene hydroclimatic change. Carbon isotopes provide complemen-
 123 tary information by recording shifts in ecosystem composition that influence the magnitude
 124 of the offsets between δD_{wax} and δD_p (Figure S1). Our approach therefore allows us to iden-
 125 tify changes in monsoon strength and spatial extent over the Plio-Pleistocene.

126 **Materials and Methods**

127 **Site Background**

128 DSDP 475 (23.05°N, 109.05°W) is located within the Gulf of California near the south-
 129 eastern edge of the peninsula of Baja California (Figure 1). Today, the site sits on a passive
 130 continental margin at a water depth of 2631 meters (Curry et al., 1982). This region of Baja
 131 California experiences northwesterly wind stress in winter and spring (Zaytsev et al., 2003).
 132 In summer, the region around DSDP 475 is influenced by northward advection of waters from
 133 the eastern Pacific warm pool (Zaytsev et al., 2003; Durazo & Baumgartner, 2002). The Plio-
 134 Pleistocene portion of the core from DSDP 475 is predominantly composed of hemipelagic
 135 muds, transitioning to diatomaceous muds in the mid- to early-Pliocene section, showing ev-
 136 idence of a consistent marine setting for this site from the early Pliocene through the Pleis-
 137 tocene (Curry et al., 1982). Age control primarily comes from biostratigraphic tiepoints (Brennan
 138 et al., 2022).

139 ODP 1012 (32.3°N, 118.4°W) is located on the California Margin, in the east Cortes Basin,
 140 with a water depth of 1772 m. This site experiences northwesterly wind stress year round. The
 141 sedimentary section consists of interbedded silty clay, nannofossil mixed sediment, nannofos-
 142 sil ooze (Ostertag-Henning & Stax, 2000). We sample primarily from core 1012A, with sup-
 143 plementary samples from 1012B in the late Pleistocene, to generate a composite Plio-Pleistocene
 144 record of climate change. The age model, previously published in J. LaRiviere (2007), is based
 145 on $\delta^{18}O$ of benthic foraminifera until approximately 1.8 Ma, and thereafter on biostratigraphic
 146 tiepoints (T. Herbert et al., 2001).

147 **Leaf Wax Extraction and Measurement**

148 Approximately 100 samples were processed from each of DSDP 475 and ODP 1012,
 149 so that the average time interval between samples was 40 kyr for DSDP 475 and 30 kyr for
 150 ODP 1012. Leaf waxes were processed via standard methods involving extraction of the to-
 151 tal lipid extract (TLE) and purification via column chromatography (Bhattacharya et al., 2018).
 152 Following previous work in the region, we focus our analyses on the C_{30} fatty acid, which ex-
 153 clusively derives from terrestrial plants (Bhattacharya et al., 2018).

154 Concentrations of C₃₀ FAMES, fatty acid methyl esters, were determined using a Trace
 155 1310 GC-FID, and their hydrogen and carbon isotopic composition were measured via gas chro-
 156 matography isotope ratio mass spectrometry (GC-IR-MS) using a Thermo Delta V Plus mass
 157 spectrometer coupled to a Trace 1310 GC-FID, using either a pyrolysis (H₂) or combustion
 158 reactor (CO₂). H₂ and CO₂ gases calibrated to a *n*-alkane standard (A7 mix provided by Arndt
 159 Schimmelmann at Indiana University) provided references for each analysis. An internal iso-
 160 topic standard consisting of a synthetic mix of FAMES was analyzed every 5-7 samples to mon-
 161 itor drift. Samples were run in triplicate for δD to obtain a precision better than 2‰ (1 σ), and
 162 in duplicate or triplicate for $\delta^{13}C$ to obtain a precision better than 0.2‰ (1 σ). While we ini-
 163 tially corrected for ice volume changes using a million-year smoothed version of the benthic
 164 oxygen isotope stack (Lisiecki & Raymo, 2005) following the method of (Schrug et al., 1996),
 165 this correction had a minimal influence on each record (Figure S1), and was omitted in our
 166 final analysis.

167 Inference of Precipitation δD

168 We leverage paired measurements of carbon and hydrogen isotopes of the C₃₀ fatty acid
 169 (hereafter, referred to as $\delta^{13}C_{wax}$ and δD_{wax}) to infer the hydrogen isotopic signature of pre-
 170 cipitation, or δD_p . δD_{wax} values are offset from the hydrogen isotopic signature of the en-
 171 vironmental waters, assumed to be the isotopic value of mean annual precipitation or δD_p . This
 172 apparent fractionation or ε_{p-w} varies across plant clades. Graminoids (e.g. grasses) tend to
 173 have a larger ε_{p-w} , or are more depleted relative to δD_p , than eudicots, likely reflecting dif-
 174 ferences in leaf wax biosynthesis and leaf development (Gao et al., 2014). Following previ-
 175 ous work, we use $\delta^{13}C_{wax}$ and a Bayesian mixing model (Tierney et al., 2017) to infer the
 176 proportion of waxes that come from C₄ grasses in each sample, since C₄ plants have a more
 177 enriched carbon isotopic signature than C₃ plants (Collister et al., 1994). End-member con-
 178 straints on C₄ grasses and C₃ eudicots come from modern plant waxes measured at the Arizona-
 179 Sonora Desert Museum in Tucson, AZ (Table S2, S3). These values are based on repeated mea-
 180 surement of new growth on each plant once a month for a calendar year. In order to make mea-
 181 surements more comparable to Plio-Pleistocene leaf wax carbon isotopes, modern plant $\delta^{13}C_{wax}$
 182 measurements were corrected for the Suess effect.

183 We then use the proportion of inferred C₄ vegetation to determine the appropriate ε_{p-w}
 184 to apply to a given sample. Constraints on ε_{p-w} are obtained from δD_{wax} measured on the
 185 Arizona-Sonora Desert Museum modern plants. The approach involves weighting the value
 186 of ε_{p-w} for C₃ and C₄ plants by the inferred fraction of C₃ and C₄ plants in the sample (Eq.
 187 1).

$$\varepsilon = f_{C4} \cdot \varepsilon_{C4} + (1 - f_{C4}) \cdot \varepsilon_{C3} \quad (1)$$

188 Finally, our weighted value of ε_{p-w} is used to infer δD_p (Eq. 2).

$$\delta D_{precip} = \frac{1000 + \delta D_{wax}}{(\varepsilon/1000) + 1} - 1000 \quad (2)$$

189 Because all calculations are performed in a Bayesian framework, uncertainties are prop-
 190 agated through all steps of the calculation. While our initial 1σ precision for δD_w measure-
 191 ments is 2%, 1σ uncertainty for our final estimate of δD_p is 4-6%. This Bayesian approach
 192 has been previously used to study paleohydrological signals in leaf waxes (Tierney et al., 2017;
 193 Windler et al., 2021), including within the NAM domain (Bhattacharya et al., 2018).

194 SST Compilation

195 To identify relationships between leaf wax-inferred δD_p and Plio-Pleistocene changes
 196 in large-scale circulation over the north Pacific, we compiled available continuous alkenone-
 197 based records of Plio-Pleistocene temperatures from the northeast Pacific. Records were cal-
 198 ibrated using BAYSPLINE, a Bayesian calibration that accounts for the attenuation of the re-
 199 lationship between the alkenone unsaturation index and temperature at warmer temperatures
 200 (Tierney & Tingley, 2018).

201 We calculate three indices of Plio-Pleistocene SSTs. First, we calculate average eastern
 202 equatorial Pacific SST by taking the mean SST anomaly of sites in the eastern equatorial Pa-
 203 cific including sites IODP U1337, ODP 847, ODP 846, and ODP 1239 (Liu et al., 2019; Dekens
 204 et al., 2007; Seki et al., 2012; Rousselle et al., 2013; Shaari et al., 2013; Etourneau et al., 2010;
 205 T. D. Herbert et al., 2016; Lawrence et al., 2006). We also exclude the lower resolution record
 206 from IODP U1338, although the choice to include or omit this record does not significantly
 207 alter our results. Next, we calculate average southern California margin SSTs by taking the
 208 average anomaly at sites ODP 1012, ODP 1014, and ODP 1010 (J. P. LaRiviere et al., 2012;
 209 J. LaRiviere, 2007; Brierley et al., 2009b; Dekens et al., 2007), also excluding sites with alkenone
 210 records that do not extend to 3.6 Ma (e.g. site 475). Finally, we calculate an index of the sub-
 211 tropical/tropical gradient in the eastern Pacific by subtracting tropical eastern equatorial Pa-
 212 cific SSTs from subtropical southern California Margin SST. This index helps quantify the *rel-*
 213 *ative* warmth on the southern California margin, and is between -7°C and -8°C in the present-
 214 day climatology.

215 **Isotope-Enabled Model Simulations**

216 To investigate the drivers of SWNA δD_p changes during the Pliocene, we analyzed sim-
 217 ulations conducted with the isotopologue-tracking enabled Community Earth System Model
 218 1.2 (iCESM1.2) in atmosphere-only mode (e.g. iCAM5) (Brady et al., 2019). The atmospheric
 219 model is run at a $0.9^\circ \times 1.25^\circ$ horizontal resolution, with 30 vertical layers. The pre-industrial
 220 simulation of iCESM1.2 used in this study captures a similar seasonal cycle of water isotopes
 221 compared to GNIP observations, with an enriched summer monsoon compared to depleted win-
 222 ter rainfall (Figure S6), despite the fact that iCESM1.2's rainfall isotopes are depleted com-
 223 pared to observations at Tucson's GNIP station (Nusbaumer et al., 2017). In addition, iCAM5
 224 performs slightly better than other models at simulating rainfall isotope changes due to chang-
 225 ing stratiform fraction (Hu et al., 2018).

226 We prescribe the idealized SST field used in Fu et al. (2022), which is based on the PRISM3
 227 SST reconstruction (Dowsett et al., 2009), but increases temperatures on the southern Cali-
 228 fornia Margin to match proxy evidence. All other boundary conditions (e.g. topography, land
 229 surface conditions), including CO_2 , are kept at pre-industrial values. This simplified experi-
 230 mental design allows us to cleanly isolate the influence of an altered SST field on SWNA hy-
 231 droclimate.

232 We also perform 6 additional iCAM5 simulations with different SST patterns and Pliocene
 233 boundary conditions in order to better understand the drivers of NAM changes. These sim-
 234 ulations featured two types of experiments: in one, we uniformly warm global SSTs without
 235 changing the subtropical/tropical gradient in the eastern Pacific. In the other, we incrementally
 236 reduce the subtropical/tropical gradient by warming the CA coast. These two sets of exper-
 237 iments identify whether uniform warming of the tropical/subtropical ocean, or alternatively,
 238 a changing warming pattern, is more important for driving NAM changes, and should be re-
 239 garded as sensitivity tests. Simulations are run for 40 years and the last 20 years of model runs
 240 are averaged to generate climatologies. It should also be noted that all simulations have fixed
 241 atmospheric CO_2 concentrations at Pliocene levels of 400 ppm, resulting in a warmer tropo-
 242 sphere with higher evaporative demand. For further details, see Text S1 and Table S4.

243 **Results and Discussion**

244 **Plio-Pleistocene Trajectory of δD_p in SWNA**

245 Our new leaf wax-based reconstructions of δD_p indicate a large shift in SWNA hydro-
 246 climate between 3.0 and 2.4 Ma, right at the Plio-Pleistocene transition and coinciding with
 247 the intensification of Northern Hemisphere glaciation (Figure 1). At site 1012, δD_p is ca. -20
 248 to -40‰ between 3.5 and 3.0 Ma and then declines to ca. -50 to -60‰ by 2.5 Ma. Af-

249 ter this point, δD_p fluctuates between -65 and -45% . A similar pattern of change is recorded
 250 at DSDP 475. At this site, Pliocene values of δD_p range between -45 and -35% , 20 to 35‰
 251 more enriched than late Pleistocene values. The most enriched values of δD_p occur between
 252 3.5 and 2.9 Ma (Figure 1), after which inferred δD_p values progressively decline until 2.4 Ma.
 253 Thereafter, values of δD_p at site 475 show an increase in variability. The increase in variabil-
 254 ity in the Pleistocene portion of both records likely reflect glacial-interglacial variability. South-
 255 ward shifts in the westerlies during glacial periods weaken the NAM by promoting ‘ventila-
 256 tion’ or the import of cold, dry air into the monsoon domain (Bhattacharya et al., 2018).

257 The similar trajectory of δD_p change over the Plio-Pleistocene transition at both sites
 258 suggests that our δD_p reconstructions reflect large-scale reorganizations of hydroclimate rather
 259 than any local topographic effects. Furthermore, independent evidence suggests that topogra-
 260 phy in western North America was already sufficiently high to establish modern circulation
 261 patterns and block Gulf of Mexico moisture, making it unlikely that Pliocene δD_p changes re-
 262 flect an increasing contribution of easterly moisture sources from the Atlantic to coastal re-
 263 gions of Baja and southern California (Mix et al., 2019; Wheeler et al., 2016).

264 We interpret the enrichment of δD_p in the Pliocene relative to late Pleistocene values
 265 as reflecting a greater proportion of convective summer rainfall during this epoch. Summer
 266 monsoon rainfall forms from vapor that is rapidly lifted from a warm, saturated boundary in
 267 strong convective updrafts (Text S2; Figure S2). This results in an enriched isotopic signature
 268 relative to winter moisture, which primarily derives from stratiform precipitation (Aggarwal
 269 et al., 2016) (Figure S2). Thus, intervals in time with enhanced deep convective and monsoon
 270 rainfall exhibit more enriched values of δD_p . This interpretation differs from the so-called ‘amount-
 271 effect’ observed in other parts of the tropics, and instead reflects the distinct climatology of
 272 the NAM region, which features a high proportion of stratiform rainfall in comparison to other
 273 monsoon regions (e.g. the Indian monsoon) (Schumacher & Houze, 2003).

274 Further support for the view that fluctuations in δD_p reflect proportions of convective
 275 and stratiform rainfall comes from the fact that spatial gradients in modern coretop leaf wax-
 276 inferred δD_p in the Gulf of California show a strong positive correlation with the fraction of
 277 rainfall derived from deep convection (Figure S2). Increasing proportions of deep convection
 278 in the region stretching from Baja California to the southern California margin can therefore
 279 explain a more positive leaf wax δD_p signature during the Pliocene. This complements the ar-
 280 gument made in Bhattacharya et al. (2018), who found that δD_p reflects changing proportions
 281 of summer and winter rainfall: summer rainfall is primarily deep convective and winter/spring
 282 rainfall derives from stratiform rain (Figure S2). Other processes, like equilibrium tempera-
 283 ture effects, are too small to explain the full magnitude of the δD changes (see Text S2).

284 In the present climatology, the region around DSDP 475 receives less than 1 mm/day
 285 of rain on average, and in many years receives no monsoon rainfall (Fonseca-Hernandez et al.,
 286 2021) (Figure S3). A positive Pliocene leaf wax δD_p signature at DSDP 475 likely reflects
 287 intensification of the monsoon in its core region, on the slopes of the Sierra Madre Occiden-
 288 tal, as well as its expansion into Baja. Similarly, the majority of rain at ODP 1012 in the present
 289 day derives from winter moisture, with virtually no contribution from summertime rainfall. The
 290 enriched signature of δD_p in the Pliocene at site 1012 reflects a fundamentally different cli-
 291 matology, with a greater proportion of summer rainfall. The similarity of the pattern between
 292 DSDP 475 and ODP 1012 suggests that the latter site reflects the expansion of the NAM
 293 into southern California in the Pliocene. This coheres with existing qualitative inferences from
 294 southern California palynological data and faunal remains, which suggest that the Pleistocene
 295 marked a transition from summer-wet to summer-dry environments in both southern Califor-
 296 nia and Baja California, (Miller, 1980; Ballog & Malloy, 1981; Axelrod, 1948). Together, these
 297 lines of evidence suggest that the Pliocene featured a stronger North American Monsoon that
 298 was spatially more extensive, influencing the entire region stretching from Baja California through
 299 southern California. Moreover, evidence for a warmer and wetter climate in the NAM region
 300 is also shown by paleo-botanical evidence from the Miocene (M. J. Pound et al., 2012), sug-
 301 gesting that other warm climate intervals in Earth history also featured a stronger NAM.

302 **SST Patterns and Plio-Pleistocene Monsoon Changes**

303 A recent modeling study hypothesized that warmer California margin temperatures in
 304 the Pliocene resulted in expanded and enhanced summer convection (Fu et al., 2022). This hy-
 305 pothesis implies that the evolution of the Plio-Pleistocene NAM should track coastal temper-
 306 atures on the California Margin. In contrast, other modeling studies suggest that NAM strength
 307 responds most strongly to the *relative* warming of the subtropical eastern Pacific (e.g. Cali-
 308 fornia Margin) compared to the eastern equatorial Pacific (EEP) (Pascale et al., 2017). To as-
 309 sess the importance of each of these factors in driving NAM changes, we compare our records
 310 of summer convection to an index of the eastern Pacific subtropical/tropical temperature gra-
 311 dient, as well as an index of California margin SSTs (see Materials and Methods).

312 Our Plio-Pleistocene records of SWNA δD_p show a stronger relationship with the east-
 313 ern Pacific subtropical/tropical gradient than the absolute magnitude of warming on the CA
 314 margin (Figure 1e and f). The subtropical/tropical gradient index shows that the temperature
 315 difference between the the California Margin and the EEP was at a minimum between 3.5 and
 316 3.0 Ma, and then progressively increased between 3.0 and 2.4 Ma until reaching modern val-
 317 ues, where the southern California Margin is approximately 7.6°C cooler than the EEP (Fig-
 318 ure 1e). The largest changes in this gradient coincide temporally with the step-like transition

319 to more depleted values in both of our δD_p records (Figure 1). In contrast, southern CA mar-
 320 gin temperatures show a gradual long-term decline from 3.5 to 0.8 Ma, with no indication of
 321 a step change at the Plio-Pleistocene transition (Figure 1f).

322 CA margin temperatures and the eastern Pacific subtropical/tropical gradient index are
 323 not independent metrics, as the former is used to calculate the latter. However, the temporal
 324 evolution of SWNA δD_p more closely mirrors the trajectory of the subtropical-tropical SST
 325 gradient than CA margin temperatures alone, which supports a causal link between long-term
 326 NAM strength and this temperature gradient. We next use isotope enabled simulations to cor-
 327 roborate this observed relationship between SST patterns, NAM strength, and δD_p .

328 **NAM changes in Isotope-enabled Simulations**

329 The iCAM5 experiment with Fu et al. (2022) SSTs produces a region of positive vapor
 330 δD anomalies that are co-located with warm SST anomalies. These vapor anomalies spatially
 331 coincide with the location of enriched δD_p and a weak, convergent, cyclonic circulation pat-
 332 tern (Figure 2). This is supported by the moisture budget analysis presented in Fu et al. (2022),
 333 which found that both thermodynamic and dynamic processes contributed to rainfall changes
 334 in their simulations. Because SST anomalies in the PRISM3 dataset are muted south of Baja
 335 California, δD_p is slightly depleted in that region, differing from our record from site 475 (Fig-
 336 ure 2, Figure S5). However, this simulation still illustrates the connection between SST, va-
 337 por and precipitation δD , and summer rainfall.

338 In iCAM5, water vapor and precipitation δD act as tracers of changes in energy for con-
 339 vection. We measure the latter using equivalent potential temperature or θ_e , a thermodynamic
 340 quantity that integrates information about the temperature and moisture content of air parcels.
 341 Vertical gradients of θ_e therefore measure the potential for instability and convection. The ver-
 342 tical profile of the atmosphere over the NAM region shows that positive θ_e anomalies, which
 343 imply greater potential for convection, are co-located with increases in water vapor δD (Fig-
 344 ure 2). Warmer subtropical SSTs likely drive higher local fluxes of sensible and latent heat.
 345 In addition, the convergent circulation over these warm coastal SSTs imports moist, warm air
 346 into this region (Fu et al., 2022). These processes result in positive anomalies of θ_e , and also
 347 change the signature of δD_p by altering the isotopic signature of the moisture source from which
 348 precipitation is derived. Water vapor changes may dominate the isotopic response in iCAM5
 349 because isotope-enabled models are known to underestimate δD_p changes that result directly
 350 from changing proportions of convective rainfall (Hu et al., 2018). Therefore, the model pro-
 351 duces a smaller magnitude of change in δD_p compared to what is estimated by the proxies,
 352 although the model does overlap the 95% confidence interval of proxy-estimated δD_p change
 353 in the Pliocene at both sites.

354 Our iCAM5 simulation confirms that a stronger summer monsoon is linked to enriched
 355 δD_p and that warm temperatures along the California margin are critical for sustaining a stronger
 356 monsoon circulation. It is notable that the simulation produces an intensification of the NAM
 357 in both the core monsoon domain, as well as an expansion of the monsoon to the north and
 358 west (Figure 2), consistent with our interpretation that our leaf wax signals reflect hydrocli-
 359 mate changes associated with the NAM. However, this single simulation does not allow us to
 360 cleanly determine whether local warming on the CA margin, versus the gradient of temper-
 361 ature between the subtropical eastern Pacific and the EEP, is more important for driving an
 362 increase in summer rain. Furthermore, it is unclear whether intensification of the NAM alone
 363 could have sustained a positive balance of precipitation minus evaporation, as is implied by
 364 qualitative proxies like mesic vegetation, high lake levels, and taxa like *Crocodylus*.

365 To identify whether local CA margin SSTs or the larger subtropical/tropical SST gra-
 366 dient was responsible for the observed hydroclimatic changes, we conducted a series of sim-
 367 ulations with iCAM5 where we systematically varied SST patterns (Figure S5). Across all of
 368 the simulations, annual P-E is strongly correlated with summer P-E ($r = 0.87$, $p=0.04$), which
 369 confirms that summer precipitation is important for maintaining a year-round positive P-E bal-
 370 ance. However, we find a weak relationship between summer P-E and temperature anomalies
 371 on the southern CA margin (Figure 3a). Even when the model SST field overlaps the range
 372 of Pliocene proxy-inferred SST warming on the southern CA margin, the model does not pro-
 373 duce positive P-E, as is implied by available qualitative proxies from the Pliocene. In contrast,
 374 summer P-E shows a statistically significant relationship with the subtropical/tropical SST gra-
 375 dient (Figure 3b). Simulations that weaken this gradient to near 2°C , which is within the range
 376 of the change suggested by Pliocene proxies, produce positive annual P-E that is primarily driven
 377 by changes in summer P-E (Figure 3b). While it is possible that the model underestimates the
 378 response of P-E to SST gradients since its low resolution does not resolve realistic patterns
 379 of moist convection, these simulations provide another line of evidence suggesting that NAM
 380 strength is determined by large-scale SST gradients between the tropics and subtropics, sup-
 381 porting the analyses of Pascale et al. (2017) and our hydroclimate and SST proxy data.

382 **Implications for Current and Future Southwestern Hydroclimate**

383 Pliocene proxy evidence and model simulations underscore the strong relationship be-
 384 tween subtropical/tropical SST gradients in the east Pacific and NAM strength, with implica-
 385 tions for understanding past and future climate in this region. Given the critical importance
 386 of temperature patterns to NAM variability, climate models with significant northeast Pacific
 387 SST bias may not produce reliable future predictions (Y. Zhu et al., 2020). This may contribute
 388 to a lack of robust predictions of future changes in the NAM, which tend to be highly depen-

389 dent on model bias and resolution (Maloney et al., 2014; Meyer & Jin, 2017; Cook & Sea-
390 ger, 2013; Almazroui et al., 2021; Moon & Ha, 2020). When global SSTs are bias-corrected,
391 high-resolution models produce robust decreases in rainfall across all seasons in response to
392 warming (Pascale et al., 2017, 2018), at odds with previous work (Meyer & Jin, 2017; Cook
393 & Seager, 2013). This result is due in part to *reduced* California margin warming compared
394 to the tropical eastern Pacific (Pascale et al., 2017; He et al., 2020). In contrast, our results
395 suggest that the Pliocene featured *enhanced* California margin warming compared to the trop-
396 ical eastern Pacific, amplifying monsoon strength. This enhanced warming in Pliocene sim-
397 ulations may reflect the long-term influence of Earth system processes related to the cryosphere
398 and vegetation, or long-term adjustments of deep ocean dynamics that alter SST patterns (Tierney
399 et al., 2019; Feng et al., 2020; Brennan et al., 2022; A. Fedorov et al., 2013; Ford et al., 2015).
400 In fact, a growing body of literature suggests that the *equilibrium* response of SST and hy-
401 droclimate to greenhouse boundary conditions, especially those that involve long-term Earth
402 system feedbacks as likely occurred during the Pliocene, may differ fundamentally from re-
403 sponses to *transient* warming (Sniderman et al., 2019; Zappa et al., 2020; Burls & Fedorov,
404 2017; Feng et al., 2022).

405 Moreover, we are able to identify events in the observational record with amplified mon-
406 soon rainfall that parallel the mechanism of monsoon intensification in the Pliocene. Since the
407 mid-20th century, the northeast Pacific has experienced multi-season or multi-year marine heat
408 waves (MHW) (Myers et al., 2018; Amaya et al., 2020; Hoegh-Guldberg et al., 2014). The
409 peak of a heat wave between 2012 and 2014 occurred in summer 2014 and featured SSTs 1-
410 2°C warmer than average on the southern California Margin (Myers et al., 2018), in a sim-
411 ilar location to where proxies suggest the warmest mid-Pliocene temperatures occurred (Fig-
412 ure 4). During this event, eastern equatorial Pacific warming associated with a developing El
413 Niño was muted. SST anomalies off the coast of Baja reached their maximum in summer 2014
414 (Myers et al., 2018). We use reanalysis data from the North American Regional Reanalysis
415 (NARR) and the NCEP-NCAR reanalysis (Mesinger et al., 2006; Kalnay et al., 1996) to plot
416 changes in precipitation, winds, and calculate changes in equivalent potential temperature θ_e .
417 To quantify changes in deep convection, we plot changes in summertime (June - September)
418 climatological outgoing longwave radiation (OLR) over southern Baja California as well as
419 the distribution of OLR values during the heat wave (Liebmann & Smith, 1996). Lower val-
420 ues of OLR indicate cooler cloud tops and deeper convection (Figure 4).

421 Statistically significant rainfall changes occur in the core NAM domain, but also in pe-
422 ripheral regions like the Baja California Peninsula, which normally experiences atmospheric
423 subsidence and receives little monsoon rain (Figure S6) (Fonseca-Hernandez et al., 2021). This
424 is illustrated by a shift in daily summertime outgoing longwave radiation (OLR) over Baja,

425 which shows an increase to near 240–250 W/m². These values are characteristic of monsoon
 426 storms, while outlying low values represent tropical storms and hurricanes (Figure 4). This in-
 427 creased convection is partially the result of the direct thermodynamic effect of warm SSTs,
 428 but we also note the presence of stronger southerly winds along the coast of Mexico (Figure 4).
 429 Circulation changes and warm SSTs increase low level moist entropy, enhancing moist con-
 430 vection over the NAM region (Figure 4). Our results are further corroborated by previous re-
 431 search showing that extreme rainfall and flooding in southern Arizona is linked to increased
 432 precipitable water offshore of Baja, similar to what we observe during the MHW (Yang et al.,
 433 2017). Moreover, previous work found that other NE Pacific marine heat waves are associ-
 434 ated with above average soil moisture across the NAM domain (Shi et al., 2021).

435 Disentangling causality in a short instrumental record is challenging, and the cause of
 436 MHW-related SST anomalies, which result from changes in surface radiation, may differ from
 437 the cause of the California margin warming in the Pliocene, which could also involve ocean
 438 dynamical adjustments (Myers et al., 2018; Brennan et al., 2022; Ford et al., 2015; A. Fedorov
 439 et al., 2013). Despite this, there are clear parallels between our conceptual model of Pliocene
 440 NAM changes and MHW-related NAM changes. For reference, we plot the 2014 marine heat
 441 wave on Figure 3. This event stands out as featuring only modest California margin SST anoma-
 442 lies, far below the range of those inferred by Pliocene proxies. However, because this marine
 443 heat wave event was paired with weak positive temperature anomalies in the EEP, this event
 444 featured a greatly relaxed subtropical/tropical SST gradient. This example suggests that, if MHW
 445 similar to those observed in 2013-2014 continue to intensify as projected, the future may fea-
 446 ture intervals with SST patterns and circulation anomalies that are conducive to more intense,
 447 spatially expanded NAM rainfall. These extreme events in turn have important societal and
 448 ecological consequences, including potentially amplifying wildfire risk by increasing plant biomass
 449 and fuel loads, and increasing hazards from landslides associated with extreme rainfall events
 450 (Mazon et al., 2016; Demaria et al., 2019; Pascale et al., 2018).

451 **Conclusions**

452 Two novel leaf wax reconstructions of SWNA hydroclimate provide proxy evidence of
 453 intensification of the NAM, as well as expansion of its spatial footprint, during the Pliocene.
 454 Instead of solely resulting from winter rain changes, wet conditions during this epoch were
 455 at least in part driven by the summer monsoon. In fact, model simulations suggest that the ma-
 456 jority of the precipitation minus evaporation signal in the Pliocene may have been driven by
 457 summer rainfall. Both proxies and models suggest that the Pliocene expansion of summer rain-
 458 fall in SWNA is linked to the subtropical/tropical SST gradient across the eastern Pacific. These
 459 results cohere with the model experiments in Pascale et al. (2017), who posit that this gradi-

ent will play a key role in the future trajectory of the NAM. Our results are also consistent with the ‘warmer-get-wetter’ paradigm, which posits that, in warm climates, the largest rainfall changes in the subtropics and tropics should occur in regions with the highest *relative* SST warming (Xie et al., 2010). They also cohere with previous work that speculated about a linkage between eastern Pacific SSTs, atmospheric stability and NAM convection in past and future climate states (Bakun, 1990; Barron et al., 2012).

SWNA is in the midst of an intensifying megadrought, driven in part by higher temperatures that increase evaporation and reduce snowpack (Williams et al., 2022). Understanding the role of monsoon rainfall in future hydroclimate has implications for regional water resources, ecosystems, wildfire regimes, and other land surface processes. There is currently no consensus about the future trajectory of the monsoon. However, recent simulations suggest that the future will feature a weaker NAM, as a result of a reduced eastern Pacific subtropical/tropical gradient that enhances atmospheric stability over SWNA (Pascale et al., 2017). This is the opposite of what proxies suggest for the Pliocene, which featured a greatly reduced reduced subtropical/tropical gradient (Brierley et al., 2009a; A. V. Fedorov et al., 2015). One possible reason for this discrepancy is because of the timescale of response for the Pliocene vs. near-future warming: the Pliocene represents an equilibrium climate state and features SST patterns that are the result of long-term adjustments of the Earth system that have yet to emerge in transient simulations of current warming (Heede et al., 2021; Rugenstein et al., 2020).

Our analysis of the observational record also suggests that the future may be characterized by intervals of expanded monsoon rainfall. We demonstrated that marine heat waves on the southern California Margin, when coupled with muted warming in the EEP, result in a stronger monsoon. While the direct influence of CO₂ is predicted to intensify individual monsoon storms (Demaria et al., 2019; Pascale et al., 2018), marine heat waves complement this mechanism by facilitating the spatial expansion of monsoon rainfall into regions like Baja and southern California. This example raises the intriguing possibility that the subtropical/tropical SST gradient may help aid efforts to improve the seasonal predictability of NAM rainfall (Grimm et al., 2020). In models, future shifts in the strength and position of the North Pacific subtropical high are likely to weaken upwelling-favorable winds along the California margin, creating changes in mean temperatures and potentially altering the frequency of local marine heat waves (Schmidt et al., 2020; Rykaczewski et al., 2015). However, current generation models are known to underestimate the intensity and duration of marine heat waves (Plecha & Soares, 2020), suggesting that alternate model configurations, possibly featuring higher oceanic resolution, may be key to estimating future changes in California margin marine heat waves and their impact on monsoon rainfall. Clarifying the future behavior of this mechanism will have important implications for our understanding of landscape and water management, since pe-

496 riods of enhanced summer rain coupled to a warmer climate may result in higher fuel loads
 497 and fire, as well as flash flooding (Moloney et al., 2019; Yang et al., 2017).

498 Our results have implications for both past and future hydroclimate change in SWNA.
 499 Several modeling studies have shown that subtropical regions, especially eastern ocean bound-
 500 ary upwelling zones, are especially sensitive to greenhouse boundary conditions (Schneider
 501 et al., 2019; J. Zhu et al., 2019). It is therefore likely that other greenhouse climate intervals
 502 witnessed similar hydroclimate reorganizations on land areas near upwelling zones. The mech-
 503 anism we identify is also relevant to the present day, since we found evidence of an expanded
 504 monsoon during the modern 2014 marine heat wave. These results underscore the fact that far
 505 from representing a climate state fundamentally dissimilar from present day, the Pliocene can
 506 both help test fundamental theories about the dynamics that govern regional circulation, and
 507 serve as an analog for the processes that will drive hydroclimate in a warmer world. Further
 508 studies of the Pliocene and similar greenhouse intervals could therefore provide key lessons
 509 relevant for adapting to both near-future and long-term regional hydroclimate changes.

510 **Data Availability Statement**

511 Newly generated datasets from DSDP 475 and ODP 1012 are available on the NOAA/NCEI
 512 Paleoclimatology Database at Bhattacharya et al. (2022b). New isotope-enabled simulations with
 513 iCAM5 have also been archived in public repositories. Consistent with Fu et al. (2022), iCAM5
 514 simulations using fixed SSTs from that paper have been archived at the Open Science Frame-
 515 work (OSF) and can be found at Bhattacharya et al. (2022c). iCAM5 simulations associated
 516 with the fixed SST sensitivity experiments in this paper are available in Zenodo and can be
 517 found at Bhattacharya et al. (2022a). The North American Regional Reanalysis can be accessed
 518 at <https://www.ncei.noaa.gov/products/weather-climate-models/north-american-regional>. Model code for isotope-enabled CESM can be obtained at <https://github.com/NCAR/iCESM1.2>.
 520

521 **Conflict of Interest**

522 The authors declare no conflicts of interest relevant to this study.

523 **Acknowledgments**

524 TB acknowledges funding support from NSF Grants Paleo Perspectives on Climate Change
 525 (P2C2) OCE-1903148 and OCE-2103015. Measurements were made possible with support from
 526 NSF MRI Grant EAR-2018078 to TB. MF was supported by the NSF Climate Dynamics pro-
 527 gram (joint NSF/NERC) grant AGS-1924538. JET acknowledges funding support from NSF
 528 OCE-1651034 and OCE-1903171. NJB and SK acknowledge funding support from NSF award

529 AGS-1844380. RF acknowledges funding from NSF Grants OCE-2103055 and OCE-1903650.
530 All simulations were conducted on Computational and Information Systems Laboratory. 2019.
531 Cheyenne: HPE/SGI ICE XA System (Climate Simulation Laboratory). Boulder, CO: National
532 Center for Atmospheric Research. doi:10.5065/D6RX99HX. We thank lab managers Patrick
533 Murphy at the University of Arizona and Jillian Aluisio and Stephanie Bullinger at Syracuse
534 University for assistance with the leaf wax analysis, and Debbie Colodner, Amy Orchard, and
535 the Junior Docents from The Arizona-Sonora Desert Museum for assisting with the collection
536 of modern desert plants.

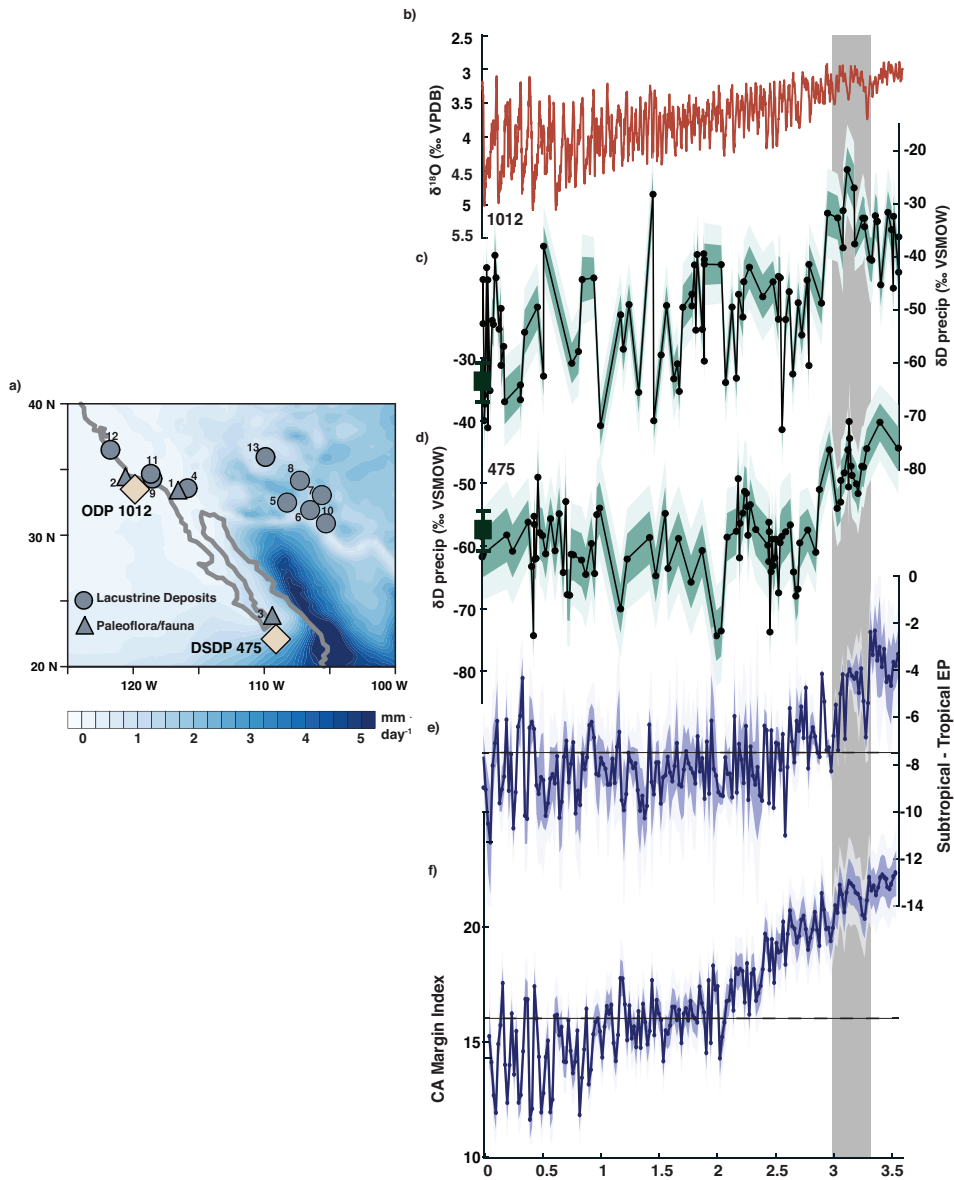


Figure 1. Plio-Pleistocene changes in SWNA hydroclimate. a) Climatological summertime precipitation across the SWNA (Mesinger et al., 2006), the locations of qualitative proxies indicating wetter conditions during the Pliocene (see Table S1), and the locations of the cores investigated in this study (ODP 1012 and DSDP 475). b) Benthic oxygen isotope stack from (Lisiecki & Raymo, 2005). c) and d) New Plio-Pleistocene reconstructions of δD_p from ODP 1012 and DSDP 475 respectively. Modern coretop values are shown as dark green squares with 1σ -error bars. e) Index of subtropical minus tropical eastern Pacific sea-surface temperature. f) Index of Plio-Pleistocene CA margin sea-surface temperature.

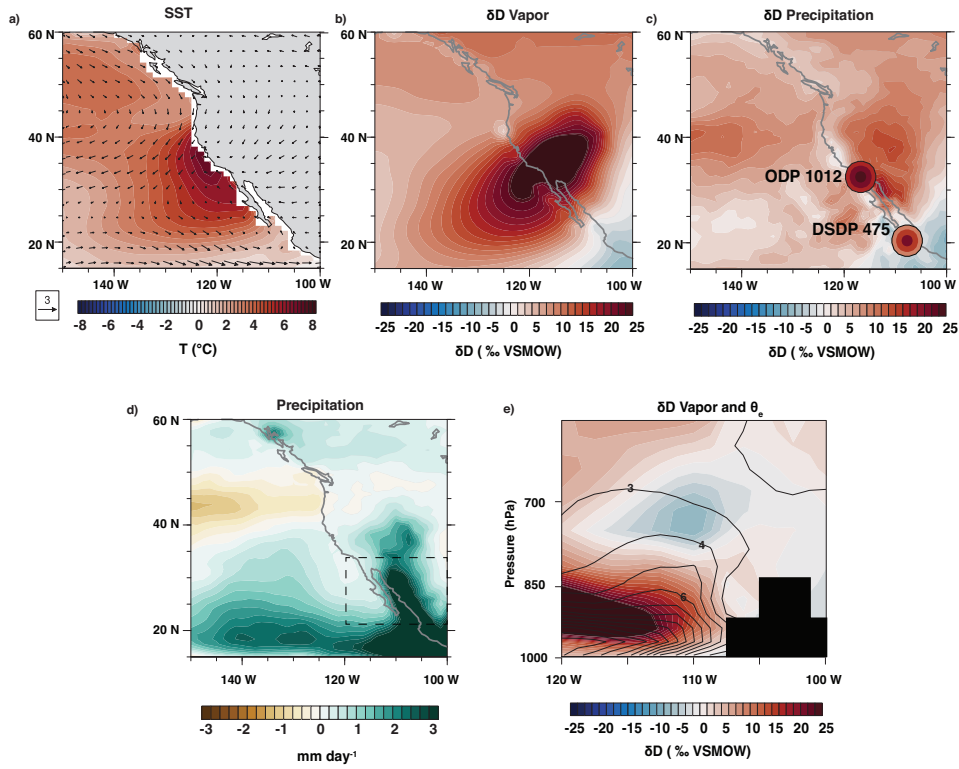


Figure 2. Summer rainfall and water isotopes in an isotope-enabled simulation forced with idealized SST changes (Fu et al., 2022). a) June-September SST and 850 mb wind anomalies. b) Vertically integrated δD of water vapor anomalies. c) δD_p anomalies, with lower (outer circle), median (middle circle), and upper (inner circle) 95% confidence interval of proxy-estimated δD_p changes at site 475 and 1012. d) Precipitation anomalies. e) The vertical profile of lower-atmospheric changes in δD of vapor and θ_e in the dashed box shown in panel d). Black outline masks areas that are below the land surface in this model.

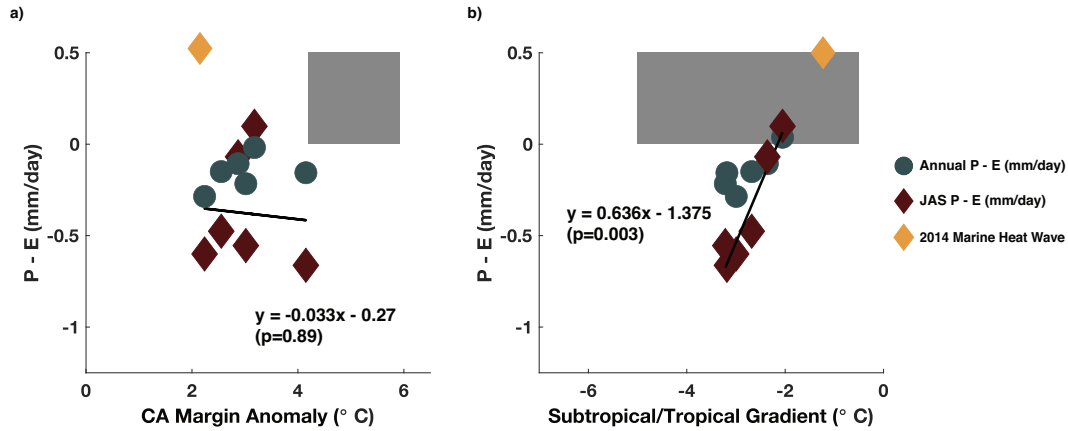


Figure 3. Relationship between SST patterns and SWNA hydroclimate in iCAM5 simulations. Red diamonds indicate changes in summer precipitation minus evaporation (P-E, mm/day); blue-green circles indicate annual P-E. a) The relationship between southern CA margin SST anomalies (SST changes between 20-35°N and 125-110°W) and P-E across SWNA (land areas between 20-35°N and 120-105°W) and P-E across SWNA (land areas between 20-35°N and 120-105°W). Gray box shows 95% confidence interval of proxy-inferred southern CA margin warming, and is located above 0 P-E since qualitative proxies (lake level, flora/fauna) suggest positive anomalies of P-E during the Pliocene. b) the relationship between the subtropical/tropical gradient and P-E. The SST gradient is calculated by taking the CA margin SST anomalies in a) and subtracting EEP temperatures (averaged between 5°S - 5°N and 170-90°W). Gray box shows proxy-inferred range of this gradient. For reference, SST and summertime P-E anomalies for the 2014 marine heat wave results presented in Figure 4 are shown as yellow diamonds.

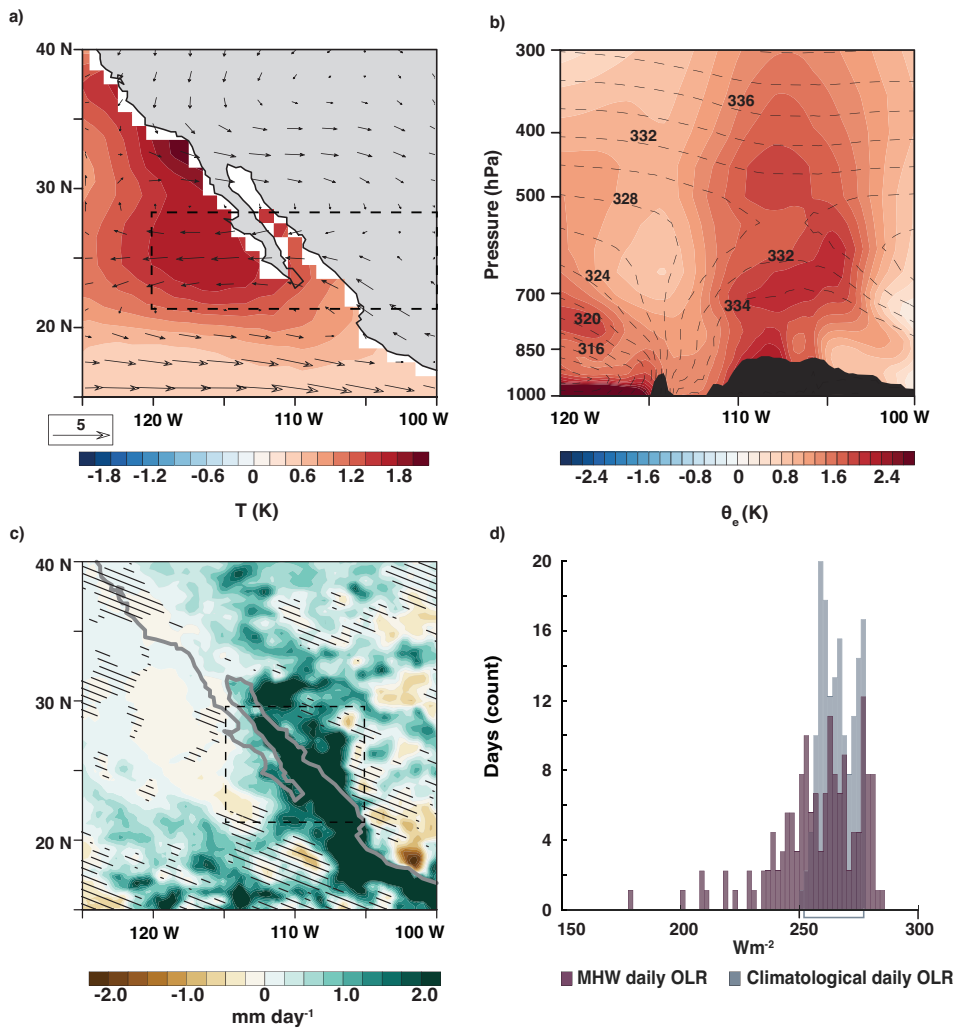


Figure 4. NAM changes during the peak of the 2014 northeast Pacific MHW. a) SST anomalies during summer 2014, the peak of the MHW, with dashed box showing location of vertical profile in panel b). b) Vertical atmospheric profile of moist entropy (θ_e) changes over Baja California in box shown in panel c). Dashed contours show climatological values, while colored contours indicate 2014 MHW anomalies. c) Rainfall anomalies in the North American Regional Analysis, with stippling showing values that are not significant at the 95% level. d) The daily distribution of climatological (gray) and MHW (purple) summertime outgoing longwave radiation (OLR). Lower OLR values indicate cooler cloud tops on deep convective clouds. Gray bracket shows 95% CI for climatological values.

537 **References**

- 538 Aggarwal, P. K., Romatschke, U., Araguas-Araguas, L., Belachew, D., Longstaffe, F. J.,
 539 Berg, P., . . . Funk, A. (2016). Proportions of convective and stratiform precipitation
 540 revealed in water isotope ratios. *Nature Geoscience*, *9*(8), 624–629.
- 541 Almazroui, M., Islam, M. N., Saeed, F., Saeed, S., Ismail, M., Ehsan, M. A., . . . others
 542 (2021). Projected changes in temperature and precipitation over the United States,
 543 Central America, and the Caribbean in CMIP6 GCMs. *Earth Systems and Environ-*
 544 *ment*, *5*(1), 1–24.
- 545 Amaya, D. J., Miller, A. J., Xie, S.-P., & Kosaka, Y. (2020). Physical drivers of the summer
 546 2019 North Pacific marine heatwave. *Nature communications*, *11*(1), 1–9.
- 547 Axelrod, D. I. (1948). Climate and evolution in western North America during middle
 548 Pliocene time. *Evolution*, 127–144.
- 549 Bakun, A. (1990). Global climate change and intensification of coastal ocean upwelling. *Sci-*
 550 *ence*, *247*(4939), 198–201.
- 551 Ballog, R. A., & Malloy, R. E. (1981). *Neogene Palynology from the Southern Califor-*
 552 *nia Continental Borderland, Site 467, Deep Sea Drilling Project Leg 64* (Vol. 63). U.S.
 553 Government Printing Office.
- 554 Barron, J. A., Metcalfe, S. E., & Addison, J. A. (2012). Response of the North American
 555 monsoon to regional changes in ocean surface temperature. *Paleoceanography*, *27*(3).
- 556 Bhattacharya, T., Feng, R., Tierney, J., Rubbelke, N., C. and Burls, Knapp, S., & Fu, M.
 557 (2022a). Expansion and intensification of the north american monsoon during the
 558 pliocene[dataset]. *Zenodo*. Retrieved from [https://doi.org/10.5281/](https://doi.org/10.5281/zenodo.7036092)
 559 [zenodo.7036092](https://doi.org/10.5281/zenodo.7036092)
- 560 Bhattacharya, T., Feng, R., Tierney, J., Rubbelke, N., C. and Burls, Knapp, S., & Fu, M.
 561 (2022b). Hydrogen isotopic reconstruction of north american monsoon since
 562 mid-pliocene [dataset]. *NOAA/NCEI Paleoclimatology Database*. Retrieved from
 563 <https://www.ncei.noaa.gov/access/paleo-search/study/36778>
- 564 Bhattacharya, T., Feng, R., Tierney, J., Rubbelke, N., C. and Burls, Knapp, S., & Fu, M.
 565 (2022c). Isotope enabled simulations for expansion and intensification of the north
 566 american monsoon during the pliocene [dataset]. *Open Science Framework*. Retrieved
 567 from <https://doi.org/10.17605/OSF.IO/REWJ5>
- 568 Bhattacharya, T., Tierney, J. E., Addison, J. A., & Murray, J. W. (2018). Ice-sheet modula-
 569 tion of deglacial North American monsoon intensification. *Nature Geoscience*, *11*(11),
 570 848–852.
- 571 Brady, E., Stevenson, S., Bailey, D., Liu, Z., Noone, D., Nusbaumer, J., . . . others (2019).
 572 The connected isotopic water cycle in the Community Earth System Model version 1.
 573 *Journal of Advances in Modeling Earth Systems*, *11*(8), 2547–2566.

- 574 Brennan, P. R., Bhattacharya, T., Feng, R., Tierney, J. E., & Jorgensen, E. (2022). Pat-
 575 terns and mechanisms of northeast pacific temperature response to pliocene boundary
 576 conditions. *Paleoceanography and Paleoclimatology*, *37*(7), e2021PA004370.
- 577 Brierley, C. M., Fedorov, A. V., Liu, Z., Herbert, T. D., Lawrence, K. T., & LaRiviere, J. P.
 578 (2009a). Greatly expanded tropical warm pool and weakened Hadley circulation in the
 579 early Pliocene. *Science*, *323*(5922), 1714–1718.
- 580 Brierley, C. M., Fedorov, A. V., Liu, Z., Herbert, T. D., Lawrence, K. T., & LaRiviere, J. P.
 581 (2009b, March). Greatly Expanded Tropical Warm Pool and Weakened Hadley Circu-
 582 lation in the Early Pliocene. *Science*, *323*(5922), 1714–1718. Retrieved 2021-05-02,
 583 from <https://science.sciencemag.org/content/323/5922/1714>
 584 (Publisher: American Association for the Advancement of Science Section: Report)
 585 doi: 10.1126/science.1167625
- 586 Burls, N. J., & Fedorov, A. V. (2017). Wetter subtropics in a warmer world: Contrasting
 587 past and future hydrological cycles. *Proceedings of the National Academy of Sciences*,
 588 *114*(49), 12888–12893.
- 589 Byrne, M. P., & O’Gorman, P. A. (2015). The response of precipitation minus evapotran-
 590 spiration to climate warming: Why the “wet-get-wetter, dry-get-drier” scaling does not
 591 hold over land. *Journal of Climate*, *28*(20), 8078–8092.
- 592 Collister, J. W., Rieley, G., Stern, B., Eglinton, G., & Fry, B. (1994). Compound-specific δ
 593 ^{13}C analyses of leaf lipids from plants with differing carbon dioxide metabolisms. *Or-*
 594 *ganic geochemistry*, *21*(6-7), 619–627.
- 595 Cook, B. I., & Seager, R. (2013). The response of the North American Monsoon to increased
 596 greenhouse gas forcing. *Journal of Geophysical Research: Atmospheres*, *118*(4),
 597 1690–1699.
- 598 Curray, J., Moore, D., Aguayo, J., Aubry, M.-P., Einsele, G., Fornari, D., . . . Vacquier,
 599 V. (1982). *Baja California Passive Margin Transect: Sites 474, 475, and 476*
 600 (Vol. 64). U.S. Government Printing Office. Retrieved 2021-04-06, from [http://](http://deepseadrilling.org/64/dsdp-toc.htm)
 601 deepseadrilling.org/64/dsdp-toc.htm doi: 10.2973/dsdp.proc.64.1982
- 602 Dekens, P. S., Ravelo, A. C., & McCarthy, M. D. (2007). Warm upwelling
 603 regions in the Pliocene warm period. *Paleoceanography*, *22*(3). Re-
 604 trieved 2021-04-06, from <http://agupubs.onlinelibrary>
 605 [.wiley.com/doi/abs/10.1029/2006PA001394](http://agupubs.onlinelibrary.wiley.com/doi/abs/10.1029/2006PA001394) (eprint:
 606 <https://onlinelibrary.wiley.com/doi/pdf/10.1029/2006PA001394>) doi: [https://doi.org/](https://doi.org/10.1029/2006PA001394)
 607 [10.1029/2006PA001394](https://doi.org/10.1029/2006PA001394)
- 608 Demaria, E. M., Hazenberg, P., Scott, R. L., Meles, M. B., Nichols, M., & Goodrich, D.
 609 (2019). Intensification of the North American Monsoon rainfall as observed from
 610 a long-term high-density gauge network. *Geophysical Research Letters*, *46*(12),

- 6839–6847.
- 611
- 612 Dowsett, H., Robinson, M., & Foley, K. (2009). Pliocene three-dimensional global ocean
613 temperature reconstruction. *Climate of the Past*, 5(4), 769–783.
- 614 Durazo, R., & Baumgartner, T. (2002). Evolution of oceanographic conditions off Baja Cali-
615 fornia: 1997–1999. *Progress in Oceanography*, 54(1-4), 7–31.
- 616 Etourneau, J., Schneider, R., Blanz, T., & Martinez, P. (2010, August). Intensification of the
617 Walker and Hadley atmospheric circulations during the Pliocene–Pleistocene climate
618 transition. *Earth and Planetary Science Letters*, 297(1), 103–110. Retrieved 2021-05-
619 02, from [https://www.sciencedirect.com/science/article/pii/](https://www.sciencedirect.com/science/article/pii/S0012821X10003845)
620 [S0012821X10003845](https://www.sciencedirect.com/science/article/pii/S0012821X10003845) doi: 10.1016/j.epsl.2010.06.010
- 621 Fedorov, A., Brierley, C., Lawrence, K. T., Liu, Z., Dekens, P., & Ravelo, A. (2013). Patterns
622 and mechanisms of early Pliocene warmth. *Nature*, 496(7443), 43–49.
- 623 Fedorov, A. V., Burls, N. J., Lawrence, K. T., & Peterson, L. C. (2015). Tightly linked zonal
624 and meridional sea surface temperature gradients over the past five million years. *Nature*
625 *Geoscience*, 8(12), 975–980.
- 626 Feng, R., Bhattacharya, T., Otto-Bliesner, B. L., Brady, E. C., Haywood, A. M., Tindall,
627 J. C., . . . others (2022). Past terrestrial hydroclimate sensitivity controlled by earth
628 system feedbacks. *Nature Communications*, 13(1), 1–11.
- 629 Feng, R., Otto-Bliesner, B. L., Brady, E. C., & Rosenbloom, N. (2020). Increased climate
630 response and earth system sensitivity from CCSM4 to CESM2 in mid-Pliocene simu-
631 lations. *Journal of Advances in Modeling Earth Systems*, 12(8), e2019MS002033.
- 632 Fonseca-Hernandez, M., Turrent, C., Mayor, Y. G., & Tereshchenko, I. (2021). Using ob-
633 servational and reanalysis data to explore the southern Gulf of California boundary
634 layer during the North American Monsoon onset. *Journal of Geophysical Research:*
635 *Atmospheres*, 126(7), e2020JD033508.
- 636 Ford, H. L., Ravelo, A. C., Dekens, P. S., LaRiviere, J. P., & Wara, M. W. (2015). The evo-
637 lution of the equatorial thermocline and the early Pliocene El Padre mean state. *Geo-*
638 *physical Research Letters*, 42(12), 4878–4887.
- 639 Fu, M., Cane, M. A., Molnar, P., & Tziperman, E. (2022, January). Warmer Pliocene up-
640 welling site SST leads to wetter subtropical coastal areas: a positive feedback on SST.
641 *Paleoceanography and Paleoclimatology*, e2021PA004357.
- 642 Gao, L., Edwards, E. J., Zeng, Y., & Huang, Y. (2014). Major evolutionary trends in hydro-
643 gen isotope fractionation of vascular plant leaf waxes. *PloS one*, 9(11), e112610.
- 644 Grimm, A. M., Dominguez, F., Cavalcanti, I. F., Cavazos, T., Gan, M. A., Silva Dias, P. L.,
645 . . . Barreiro, M. (2020). South and North American Monsoons: Characteristics, life
646 cycle, variability, modeling, and prediction. In *The multiscale global monsoon system*
647 (pp. 49–66). World Scientific.

- 648 He, C., Li, T., & Zhou, W. (2020). Drier North American monsoon in contrast to Asian–
649 African monsoon under global warming. *Journal of Climate*, *33*(22), 9801–9816.
- 650 Heede, U. K., Fedorov, A. V., & Burls, N. J. (2021). A stronger versus weaker Walker:
651 understanding model differences in fast and slow tropical Pacific responses to global
652 warming. *Climate Dynamics*, *57*(9), 2505–2522.
- 653 Herbert, T., Schuffert, J., Andreasen, D., Heusser, L., Lyle, M., Mix, A., . . . Herguera, J.
654 (2001). Collapse of the California current during glacial maxima linked to climate
655 change on land. *Science*, *293*(5527), 71–76.
- 656 Herbert, T. D., Lawrence, K. T., Tzanova, A., Peterson, L. C., Caballero-Gill, R., & Kelly,
657 C. S. (2016, November). Late Miocene global cooling and the rise of modern
658 ecosystems. *Nature Geoscience*, *9*(11), 843–847. Retrieved 2021-05-02, from
659 <https://www.nature.com/articles/ngeo2813> (Number: 11 Publisher:
660 Nature Publishing Group) doi: 10.1038/ngeo2813
- 661 Hoegh-Guldberg, O., Cai, R., Poloczanska, E., Brewer, P., Sundby, S., Hilmi, K., . . . Jung,
662 S. (2014). *The ocean. in: Climate change 2014: Impacts, adaptation, and vulnerabil-*
663 *ity. part b: Regional aspects. contribution of working group ii to the fifth assessment*
664 *report of the intergovernmental panel on climate change.* Intergovernmental Panel on
665 Climate Change.
- 666 Hu, J., Emile-Geay, J., Nusbaumer, J., & Noone, D. (2018). Impact of convective activity on
667 precipitation δ 18O in isotope-enabled general circulation models. *Journal of Geophys-*
668 *ical Research: Atmospheres*, *123*(23), 13–595.
- 669 Ibarra, D. E., Oster, J. L., Winnick, M. J., Caves Rügenstein, J. K., Byrne, M. P., & Chamber-
670 lain, C. P. (2018). Warm and cold wet states in the western United States during the
671 Pliocene–Pleistocene. *Geology*, *46*(4), 355–358.
- 672 Kalnay, E., Kanamitsu, M., Kistler, R., Collins, W., Deaven, D., Gandin, L., . . . Joseph, D.
673 (1996). The ncep/ncar 40-year reanalysis project. *Bulletin of the American meteor-*
674 *ological Society*, *77*(3), 437–472.
- 675 LaRiviere, J. (2007). *California margin sea surface temperature and paleoproductivity*
676 *records at ocean drilling program site 1012.* Southern Illinois University at Carbon-
677 dale.
- 678 LaRiviere, J. P., Ravelo, A. C., Crimmins, A., Dekens, P. S., Ford, H. L., Lyle, M., & Wara,
679 M. W. (2012, June). Late Miocene decoupling of oceanic warmth and atmospheric
680 carbon dioxide forcing. *Nature*, *486*(7401), 97–100. Retrieved 2021-05-02, from
681 <https://www.nature.com/articles/nature11200> (Number: 7401
682 Publisher: Nature Publishing Group) doi: 10.1038/nature11200
- 683 Lawrence, K. T., Liu, Z., & Herbert, T. D. (2006, April). Evolution of the Eastern Tropical
684 Pacific Through Plio-Pleistocene Glaciation. *Science*, *312*(5770), 79–83. Retrieved

- 2021-05-12, from <https://science.sciencemag.org/content/312/5770/79> (Publisher: American Association for the Advancement of Science Section: Research Article) doi: 10.1126/science.1120395
- 685
686
687
- 688 Liebmann, B., & Smith, C. A. (1996). Description of a complete (interpolated) outgoing
689 longwave radiation dataset. *Bulletin of the American Meteorological Society*, 77(6),
690 1275–1277.
- 691 Lisiecki, L. E., & Raymo, M. E. (2005). A Pliocene-Pleistocene stack of 57 globally dis-
692 tributed benthic $\delta^{18}\text{O}$ records. *Paleoceanography*, 20(1).
- 693 Liu, J., Tian, J., Liu, Z., Herbert, T. D., Fedorov, A. V., & Lyle, M. (2019, April). East-
694 ern equatorial Pacific cold tongue evolution since the late Miocene linked to extra-
695 tropical climate. *Science Advances*, 5(4), eaau6060. Retrieved 2021-07-11, from
696 <https://advances.sciencemag.org/content/5/4/eaau6060> (Pub-
697 lisher: American Association for the Advancement of Science Section: Research
698 Article) doi: 10.1126/sciadv.aau6060
- 699 Maloney, E. D., Camargo, S. J., Chang, E., Colle, B., Fu, R., Geil, K. L., ... others (2014).
700 North American climate in CMIP5 experiments: Part III: Assessment of twenty-first-
701 century projections. *Journal of Climate*, 27(6), 2230–2270.
- 702 Mazon, J. J., Castro, C. L., Adams, D. K., Chang, H.-I., Carrillo, C. M., & Brost, J. J. (2016).
703 Objective climatological analysis of extreme weather events in Arizona during the
704 North American monsoon. *Journal of Applied Meteorology and Climatology*, 55(11),
705 2431–2450.
- 706 Mesinger, F., DiMego, G., Kalnay, E., Mitchell, K., Shafran, P. C., Ebisuzaki, W., ... Shi, W.
707 (2006). North american regional reanalysis. *Bulletin of the American Meteorological*
708 *Society*, 87(3), 343–360.
- 709 Meyer, J. D., & Jin, J. (2017). The response of future projections of the North American
710 monsoon when combining dynamical downscaling and bias correction of CCSM4
711 output. *Climate Dynamics*, 49(1), 433–447.
- 712 Miller, W. E. (1980). The late Pliocene Las Tunas local fauna from southernmost Baja Cali-
713 fornia, Mexico. *Journal of Paleontology*, 762–805.
- 714 Mix, H. T., Rugestein, J. K. C., Reilly, S. P., Ritch, A. J., Winnick, M. J., Kukla, T., &
715 Chamberlain, C. P. (2019). Atmospheric flow deflection in the late cenozoic sierra
716 nevada. *Earth and Planetary Science Letters*, 518, 76–85.
- 717 Molnar, P., & Cane, M. A. (2002). El Niño's tropical climate and teleconnections as a
718 blueprint for pre-Ice Age climates. *Paleoceanography*, 17(2), 11–1.
- 719 Moloney, K. A., Mudrak, E. L., Fuentes-Ramirez, A., Parag, H., Schat, M., & Holzapel, C.
720 (2019). Increased fire risk in Mojave and Sonoran shrublands due to exotic species and
721 extreme rainfall events. *Ecosphere*, 10(2), e02592.

- 722 Moon, S., & Ha, K.-J. (2020). Future changes in monsoon duration and precipitation using
723 CMIP6. *npj Climate and Atmospheric Science*, 3(1), 1–7.
- 724 Myers, T. A., Mechoso, C. R., Cesana, G. V., DeFlorio, M. J., & Waliser, D. E. (2018).
725 Cloud feedback key to marine heatwave off Baja California. *Geophysical Research*
726 *Letters*, 45(9), 4345–4352.
- 727 Nusbaumer, J., Wong, T. E., Bardeen, C., & Noone, D. (2017). Evaluating hydrological
728 processes in the Community Atmosphere Model Version 5 (CAM5) using sta-
729 ble isotope ratios of water. *Journal of Advances in Modeling Earth Systems*, 9(2),
730 949–977.
- 731 Ostertag-Henning, C., & Stax, R. (2000). Data report: Carbonate records from sites 1012,
732 1013, 1017, and 1019 and alkenone-based sea-surface temperatures from site 1017. In
733 *Proc. ocean drill. program, sci. results* (Vol. 167, pp. 297–302).
- 734 Pascale, S., Boos, W. R., Bordoni, S., Delworth, T. L., Kapnick, S. B., Murakami, H., ...
735 Zhang, W. (2017). Weakening of the North American monsoon with global warming.
736 *Nature Climate Change*, 7(11), 806–812.
- 737 Pascale, S., Kapnick, S. B., Bordoni, S., & Delworth, T. L. (2018). The influence of CO₂
738 forcing on North American monsoon moisture surges. *Journal of Climate*, 31(19),
739 7949–7968.
- 740 Plecha, S. M., & Soares, P. M. (2020). Global marine heatwave events using the new cmip6
741 multi-model ensemble: from shortcomings in present climate to future projections. *En-
742 vironmental Research Letters*, 15(12), 124058.
- 743 Pound, M., Tindall, J., Pickering, S., Haywood, A., Dowsett, H., & Salzmann, U. (2014).
744 Late Pliocene lakes and soils: a global data set for the analysis of climate feedbacks in
745 a warmer world. *Climate of the Past*, 10(1), 167–180.
- 746 Pound, M. J., Haywood, A. M., Salzmann, U., & Riding, J. B. (2012). Global vegeta-
747 tion dynamics and latitudinal temperature gradients during the mid to late miocene
748 (15.97–5.33 ma). *Earth-Science Reviews*, 112(1-2), 1–22.
- 749 Remeika, P., Fischbein, I. W., & Fischbein, S. A. (1988). Lower Pliocene petrified wood
750 from the Palm Spring Formation, Anza Borrego Desert State Park, California. *Review*
751 *of palaeobotany and palynology*, 56(3-4), 183–198.
- 752 Rousselle, G., Beltran, C., Sicre, M.-A., Raffi, I., & De Rafélis, M. (2013, January).
753 Changes in sea-surface conditions in the Equatorial Pacific during the middle
754 Miocene–Pliocene as inferred from coccolith geochemistry. *Earth and Plane-
755 tary Science Letters*, 361, 412–421. Retrieved 2021-05-02, from [https://www](https://www.sciencedirect.com/science/article/pii/S0012821X12006115)
756 [.sciencedirect.com/science/article/pii/S0012821X12006115](https://www.sciencedirect.com/science/article/pii/S0012821X12006115)
757 doi: 10.1016/j.epsl.2012.11.003
- 758 Rugenstein, M., Bloch-Johnson, J., Gregory, J., Andrews, T., Mauritsen, T., Li, C., ...

- 759 Knutti, R. (2020). Equilibrium climate sensitivity estimated by equilibrating cli-
760 mate models. *Geophysical Research Letters*, *47*(4), e2019GL083898.
- 761 Rykaczewski, R. R., Dunne, J. P., Sydean, W. J., García-Reyes, M., Black, B. A., & Bo-
762 grad, S. J. (2015). Poleward displacement of coastal upwelling-favorable winds in
763 the ocean's eastern boundary currents through the 21st century. *Geophysical Research*
764 *Letters*, *42*(15), 6424–6431.
- 765 Sachse, D., Billault, I., Bowen, G. J., Chikaraishi, Y., Dawson, T. E., Feakins, S. J., . . . oth-
766 ers (2012). Molecular paleohydrology: interpreting the hydrogen-isotopic composition
767 of lipid biomarkers from photosynthesizing organisms. *Annual Review of Earth and*
768 *Planetary Sciences*, *40*, 221–249.
- 769 Salzmann, U., Haywood, A. M., & Lunt, D. J. (2009). The past is a guide to the future?
770 Comparing Middle Pliocene vegetation with predicted biome distributions for the
771 twenty-first century. *Philosophical Transactions of the Royal Society A: Mathematical,*
772 *Physical and Engineering Sciences*, *367*(1886), 189–204.
- 773 Schmidt, D. F., Amaya, D. J., Grise, K. M., & Miller, A. J. (2020). Impacts of shifting sub-
774 tropical highs on the California Current and Canary Current systems. *Geophysical Re-*
775 *search Letters*, *47*(15), e2020GL088996.
- 776 Schneider, T., Kaul, C. M., & Pressel, K. G. (2019). Possible climate transitions from
777 breakup of stratocumulus decks under greenhouse warming. *Nature Geoscience*,
778 *12*(3), 163–167.
- 779 Schrag, D. P., Hampt, G., & Murray, D. W. (1996). Pore fluid constraints on the tempera-
780 ture and oxygen isotopic composition of the glacial ocean. *Science*, *272*(5270), 1930–
781 1932.
- 782 Schumacher, C., & Houze, R. A. (2003). The TRMM precipitation radar's view of shallow,
783 isolated rain. *Journal of Applied Meteorology and Climatology*, *42*(10), 1519–1524.
- 784 Seager, R., Naik, N., & Vecchi, G. A. (2010). Thermodynamic and dynamic mechanisms
785 for large-scale changes in the hydrological cycle in response to global warming. *Jour-*
786 *nal of climate*, *23*(17), 4651–4668.
- 787 Seki, O., Schmidt, D. N., Schouten, S., Hopmans, E. C., Damsté, J. S. S., & Pancost, R. D.
788 (2012). Paleooceanographic changes in the Eastern Equatorial Pacific over the last 10
789 Myr. *Paleoceanography*, *27*(3). Retrieved 2021-05-02, from [https://agupubs](https://agupubs.onlinelibrary.wiley.com/doi/abs/10.1029/2011PA002158)
790 [.onlinelibrary.wiley.com/doi/abs/10.1029/2011PA002158](https://agupubs.onlinelibrary.wiley.com/doi/abs/10.1029/2011PA002158)
791 ([_eprint: https://agupubs.onlinelibrary.wiley.com/doi/pdf/10.1029/2011PA002158](https://agupubs.onlinelibrary.wiley.com/doi/pdf/10.1029/2011PA002158))
792 doi: <https://doi.org/10.1029/2011PA002158>
- 793 Shaari, H. b., Yamamoto, M., & Irino, T. (2013, September). Enhanced upwelling in
794 the eastern equatorial Pacific at the last five glacial terminations. *Palaeogeog-*
795 *raphy, Palaeoclimatology, Palaeoecology*, *386*, 8–15. Retrieved 2021-05-12,

- 796 from [https://www.sciencedirect.com/science/article/pii/](https://www.sciencedirect.com/science/article/pii/S0031018213001600)
 797 S0031018213001600 doi: 10.1016/j.palaeo.2013.03.022
- 798 Shi, H., García-Reyes, M., Jacox, M. G., Rykaczewski, R. R., Black, B. A., Bograd, S. J.,
 799 & Sydeman, W. J. (2021). Co-occurrence of California drought and northeast Pacific
 800 marine heatwaves under climate change. *Geophysical Research Letters*, 48(17),
 801 e2021GL092765.
- 802 Sniderman, J., Brown, J. R., Woodhead, J. D., King, A. D., Gillett, N. P., Tokarska, K. B.,
 803 ... Meinshausen, M. (2019). Southern Hemisphere subtropical drying as a transient
 804 response to warming. *Nature Climate Change*, 9(3), 232–236.
- 805 Tierney, J. E., Haywood, A. M., Feng, R., Bhattacharya, T., & Otto-Bliesner, B. L. (2019).
 806 Pliocene warmth consistent with greenhouse gas forcing. *Geophysical Research Letters*,
 807 46(15), 9136–9144.
- 808 Tierney, J. E., Pausata, F. S., & deMenocal, P. B. (2017). Rainfall regimes of the green sa-
 809 hara. *Science advances*, 3(1), e1601503.
- 810 Tierney, J. E., & Tingley, M. P. (2018). BAYSPLINE: A new calibration for the alkenone pa-
 811 leothermometer. *Paleoceanography and Paleoclimatology*, 33(3), 281–301.
- 812 Wheeler, L. B., Galewsky, J., Herold, N., & Huber, M. (2016). Late Cenozoic surface uplift
 813 of the southern Sierra Nevada (California, USA): A paleoclimate perspective on lee-side
 814 stable isotope paleoaltimetry. *Geology*, 44(6), 451–454.
- 815 Williams, A. P., Cook, B. I., & Smerdon, J. E. (2022). Rapid intensification of the emerging
 816 southwestern North American megadrought in 2020–2021. *Nature Climate Change*,
 817 1–3.
- 818 Windler, G., Tierney, J. E., & Anchukaitis, K. J. (2021). Glacial-interglacial shifts dominate
 819 tropical Indo-Pacific hydroclimate during the late Pleistocene. *Geophysical Research*
 820 *Letters*, 48(15), e2021GL093339.
- 821 Xie, S.-P., Deser, C., Vecchi, G. A., Ma, J., Teng, H., & Wittenberg, A. T. (2010). Global
 822 warming pattern formation: Sea surface temperature and rainfall. *Journal of Climate*,
 823 23(4), 966–986.
- 824 Yang, L., Smith, J., Baeck, M. L., Morin, E., & Goodrich, D. C. (2017). Flash flooding
 825 in arid/semiarid regions: Dissecting the hydrometeorology and hydrology of the 19
 826 August 2014 storm and flood hydroclimatology in Arizona. *Journal of Hydrometeorol-*
 827 *ogy*, 18(12), 3103–3123.
- 828 Zappa, G., Ceppi, P., & Shepherd, T. G. (2020). Time-evolving sea-surface warming patterns
 829 modulate the climate change response of subtropical precipitation over land. *Proceed-*
 830 *ings of the National Academy of Sciences*, 117(9), 4539–4545.
- 831 Zaytsev, O., Cervantes-Duarte, R., Montante, O., & Gallegos-García, A. (2003). Coastal
 832 upwelling activity on the Pacific shelf of the Baja California Peninsula. *Journal of*

833 *oceanography*, 59(4), 489–502.

834 Zhu, J., Poulsen, C. J., & Tierney, J. E. (2019). Simulation of Eocene extreme warmth and
835 high climate sensitivity through cloud feedbacks. *Science advances*, 5(9), eaax1874.

836 Zhu, Y., Zhang, R.-H., & Sun, J. (2020, September). North Pacific Upper-Ocean Cold
837 Temperature Biases in CMIP6 Simulations and the Role of Regional Vertical
838 Mixing. *Journal of Climate*, 33(17), 7523–7538. Retrieved 2021-12-20, from
839 [https://journals.ametsoc.org/view/journals/clim/33/17/
840 jcliD190654.xml](https://journals.ametsoc.org/view/journals/clim/33/17/jcliD190654.xml) doi: 10.1175/JCLI-D-19-0654.1

Supporting Information for “Expansion and intensification of the North American Monsoon during the Pliocene”

Tripti Bhattacharya ¹, Ran Feng ², Jessica E. Tierney ³, Claire Rubbelke ¹,
Natalie Burls ⁴, Scott Knapp ⁴, Minmin Fu ⁵

¹Department of Earth and Environmental Sciences, Syracuse University, Syracuse NY

²Department of Geosciences, University of Connecticut, Storrs CT

³Department of Geosciences, University of Arizona, Tucson AZ

⁴Department of Atmospheric, Oceanic and Earth Sciences, George Mason University, Fairfax VA

⁵Department of Earth and Planetary Sciences, Harvard University, Cambridge, MA

Contents of this file

1. Text S1
 2. Text S2
 3. References
 4. Tables S1 to S4
 5. Figures S1 to S6
-

Text S1 - Detailed Methods

iCAM5 Simulations with Fixed SSTs

To establish a linkage between precipitation isotopes, monsoon rainfall, and SST changes, we performed a simulation with the isotopologue-tracking enabled Community Earth System Model 1.2 (iCESM1.2) in atmosphere-only mode (e.g. iCAM5) (Brady et al., 2019). The atmospheric model is run at a $0.9^\circ \times 1.25^\circ$ horizontal resolution, with 30 vertical layers. While isotope-enabled models have limitations, we note that the pre-industrial simulation of iCAM5 used in this study is able capture the seasonal contrast in precipitation δD found in GNIP station data in Tucson AZ, with an enriched summer monsoon compared to depleted winter rainfall (Figure S6), despite the fact that iCESM1.2's rainfall isotopes are depleted compared to observations at Tucson's GNIP station (Nusbaumer et al., 2017). In addition, iCAM5 performs slightly better than other models at simulating rainfall isotope changes due to changing stratiform fraction (Hu et al., 2018). We therefore suggest that this model is appropriate for investigating changes in δD_p associated with Pliocene boundary conditions.

We perform one simulation using the SST field from Fu, Cane, Molnar, and Tziperman (2022), which uses reconstructed Pliocene SSTs with amplified warming on the southern California Margin. SSTs used in this simulation are shown in Figure S5, panel a. This simulation is used to diagnose the linkage between SST changes, δD_p , and summer rainfall. In this simulation, we analyze isotopes of water vapor and precipitation, and plot changes in precipitation, winds, as well as derived fields like equivalent potential temperature (θ_e).

To identify the influence of different SST patterns on NAM strength, we perform a set of 7 sensitivity experiments using iCAM5 with prescribed SST fields. All simulations use

the same Pliocene boundary conditions adapted for Community Earth System Model, and use CO₂ concentrations of 400 ppm (Feng et al., 2020). Two experiments were designed to analyze the impact of uniform warming. SSTs in these experiments are increased by 1°C and 2°C without any changes in spatial patterns (Table S4). The 1°C warming field is shown in Figure S5, panel b. This means that this experiment represents a uniform warming of 1°C *on top of* the SST anomalies from a coupled CESM1.2 simulation from (Feng et al., 2020).

Four of the experiments are designed to sample a range of SST gradient changes associated with CA coastal warming. The coastal warming pattern is derived from the pattern of SST anomalies during the 2014 western U.S. coast marine heat wave event. In order to create prescribed SSTs for the iCAM5 simulations, these SST anomalies were scaled by 1x, 2x, 3x, and 4x and added to Pliocene SST field obtained from a fully-coupled model simulation using the Community Earth System Model version 1.2 (CESM1.2) using the same boundary conditions (Feng et al., 2020). The 1x pattern from these ‘MHW-like’ experiments is shown in Figure S5, panel c. All experiments were run for 40 model years. The last 20 model years are averaged to produce climatologies. For clarity, Table S4 details each experiment’s SST design, how CA margin and the subtropical/tropical gradient vary across simulations.

Text S2 - Interpretation of Inferred δD_p

Plio-Pleistocene changes in leaf wax isotopes reflect changes in the intensity and spatial extent of moist convection over southern California and Baja California. Modern core-top samples show a more enriched value of δD_p in the southern Gulf of California, where monsoonal, convective rainfall forms a greater proportion of total rainfall (Figure S2).

Seasonal changes in precipitation isotopes, measured at a GNIP station in Tucson, also suggest that the summer months, which feature more convective rainfall, have a more enriched isotopic signature (Figure S2) (Bhattacharya et al., 2018).

Monsoon rainfall is characterized by a greater proportion of deep convection, and exhibits a more positive value of δD_p . Deep convective monsoon rainfall results from ice hydrometeors that develop when vapor evaporated in a warm, saturated boundary layer is lifted in strong updrafts, resulting in a more enriched isotopic signature for rainfall (Aggarwal et al., 2016). In contrast, stratiform rainfall tends to form in environments with relatively weak updrafts, and may develop relatively slowly, incorporating mid to upper tropospheric water vapor and undergoing more phase changes, resulting in a depleted isotopic signature (Aggarwal et al., 2016). This is opposite to the ‘amount effect,’ where more rainfall is associated with a more depleted isotopic signature (Risi et al., 2008), but is consistent with our understanding of regional isotope systematics. The NAM region differs from other tropical regions (e.g. the Asian monsoon) as it receives a substantial amount of stratiform rainfall, which likely overprints any amount effect (Schumacher & Houze, 2003). Other processes, like temperature and changes in vapor source region, may influence inferred δD_p values. However, equilibrium temperature effects (e.g. changes in the fractionation between atmospheric water vapor and rainfall) could only account for 5-7‰ of the overall change observed in δD_p values at most. SST anomalies between 3.5 and 3.0 Ma at DSDP 475 and ODP 1012 were between 4-6°C warmer than pre-industrial values, which would translate into a 4 to 6‰ change in δD_p relative to atmospheric water vapor, assuming that condensation temperatures shifted similarly to SSTs. This is

smaller than the magnitude of δD_p change at both sites, suggesting other processes are responsible for the full magnitude of the signal.

References

- Adler, R. F., Sapiano, M. R., Huffman, G. J., Wang, J.-J., Gu, G., Bolvin, D., . . . others (2018). The Global Precipitation Climatology Project (GPCP) monthly analysis (new version 2.3) and a review of 2017 global precipitation. *Atmosphere*, *9*(4), 138.
- Aggarwal, P. K., Romatschke, U., Araguas-Araguas, L., Belachew, D., Longstaffe, F. J., Berg, P., . . . Funk, A. (2016). Proportions of convective and stratiform precipitation revealed in water isotope ratios. *Nature Geoscience*, *9*(8), 624–629.
- Ballog, R. A., & Malloy, R. E. (1981). *Neogene Palynology from the Southern California Continental Borderland, Site 467, Deep Sea Drilling Project Leg 64* (Vol. 63). U.S. Government Printing Office.
- Bhattacharya, T., Tierney, J. E., Addison, J. A., & Murray, J. W. (2018). Ice-sheet modulation of deglacial North American monsoon intensification. *Nature Geoscience*, *11*(11), 848–852.
- Brady, E., Stevenson, S., Bailey, D., Liu, Z., Noone, D., Nusbaumer, J., . . . others (2019). The connected isotopic water cycle in the Community Earth System Model version 1. *Journal of Advances in Modeling Earth Systems*, *11*(8), 2547–2566.
- Eastoe, C., & Dettman, D. (2016). Isotope amount effects in hydrologic and climate

reconstructions of monsoon climates: Implications of some long-term data sets for precipitation. *Chemical Geology*, 430, 78–89.

Feng, R., Otto-Bliesner, B. L., Brady, E. C., & Rosenbloom, N. (2020). Increased climate response and earth system sensitivity from cesm4 to cesm2 in mid-pliocene simulations. *Journal of Advances in Modeling Earth Systems*, 12(8), e2019MS002033.

Fu, M., Cane, M. A., Molnar, P., & Tziperman, E. (2022, January). Warmer Pliocene upwelling site SST leads to wetter subtropical coastal areas: a positive feedback on SST. *Paleoceanography and Paleoclimatology*, e2021PA004357.

Hu, J., Emile-Geay, J., Nusbaumer, J., & Noone, D. (2018). Impact of convective activity on precipitation $\delta^{18}\text{O}$ in isotope-enabled general circulation models. *Journal of Geophysical Research: Atmospheres*, 123(23), 13–595.

Ibarra, D. E., Oster, J. L., Winnick, M. J., Caves Rügenstein, J. K., Byrne, M. P., & Chamberlain, C. P. (2018). Warm and cold wet states in the western United States during the Pliocene–Pleistocene. *Geology*, 46(4), 355–358.

Miller, W. E. (1980). The late Pliocene Las Tunas local fauna from southernmost Baja California, Mexico. *Journal of Paleontology*, 762–805.

Nusbaumer, J., Wong, T. E., Bardeen, C., & Noone, D. (2017). Evaluating hydrological processes in the Community Atmosphere Model Version 5 (CAM5) using stable isotope ratios of water. *Journal of Advances in Modeling Earth Systems*, 9(2), 949–

977.

Remeika, P., Fischbein, I. W., & Fischbein, S. A. (1988). Lower Pliocene petrified wood from the Palm Spring Formation, Anza Borrego Desert State Park, California.

Review of palaeobotany and palynology, 56(3-4), 183–198.

Risi, C., Bony, S., & Vimeux, F. (2008). Influence of convective processes on the isotopic composition ($\delta^{18}\text{O}$ and δD) of precipitation and water vapor in the tropics:

2. Physical interpretation of the amount effect. *Journal of Geophysical Research:*

Atmospheres, 113(D19).

Schumacher, C., & Houze, R. A. (2003). The TRMM precipitation radar's view of shallow, isolated rain. *Journal of Applied Meteorology and Climatology*, 42(10), 1519–1524.

Table S1. Locations and interpretations of Pliocene data shown in Figure 1

Site	Name	Lat	Lon	Age (Ma)	Interpretation	Source
1	Diablo Formation	33.26	-116.37	3.8 - 2.6	mesic plant taxa incl <i>Juglans</i> , <i>Carya</i> , <i>Umbellaria</i> , <i>Populus</i>	(Remeika et al., 1988)
2	DSDP 467	33.83	-120.75	15 - 2.4	<i>Carya</i> , <i>Juglans</i> indicate summer wet to summer dry transition	(Ballog & Malloy, 1981)
3	Las Tunas	23.3	-109.7	4.75 - 2.6	faunal remains incl. and tortoise indicate perennial freshwater, tropical environment	(Miller, 1980)
4	Palm Springs	33.57	-115.85	3.3 - 2.6	Lacustrine Deposits	Macrostrat, (Ibarra et al., 2018)
5	Gila Conglomerate	32.48	-108.26	4.0 - 2.6	Lacustrine Deposits	Macrostrat, (Ibarra et al., 2018)
6	Fort Hancock	31.91	-106.5	3.6 - 1.9	Lacustrine Deposits	Macrostrat, (Ibarra et al., 2018)
7	Santa Fe Group 1	33.05	-105.61	19.3 - 1.9	Lacustrine Deposits	Macrostrat, (Ibarra et al., 2018)
8	Santa Fe Group 2	34.15	-107.28	4.9 - 0.7	Lacustrine Deposits	Macrostrat, (Ibarra et al., 2018)
9	Sunshine Ranch/Saugus Fm	34.3	-118.53	3.1 - 2.8	Lacustrine Deposits	Macrostrat, (Ibarra et al., 2018)
10	Hueca Bolson, TX	30.90	-105.30	4.75 - 1.8	Lacustrine Deposits	Macrostrat, (Ibarra et al., 2018)
11	Hungry Valley	34.67	-118.66	4.9 - 2.6	Lacustrine Deposits	Macrostrat, (Ibarra et al., 2018)
12	Paso Robles	36.5	-121.74	1.9-8.3	Lacustrine Deposits	Macrostrat, (Ibarra et al., 2018)
13	Bidahochi	35.95	-109.91	5.3-2.6	Lacustrine Deposits	Macrostrat, (Ibarra et al., 2018)

Table S2. Individual plant taxa from the Arizona-Sonora Desert Museum of δD_{wax} and $\delta^{13}C_{wax}$ for C_4 monocots/grasses and C_3 eudicots used to infer ε_{p-w} . Values are for the C_{30} fatty acid. Graminoids/grasses are marked with an asterisk (*).

Taxon	Ecosystem	Metabolism	$\delta^{13}C_{wax}$ (‰ VPDB)	δD_{wax} (‰ VSMOW)
<i>Acacia willardiana</i>	Thornscrub	C_3	no data	-97
<i>Ambrosia ambrosoides</i>	Sonoran Desert	C_3	-35.7	-126
<i>Ambrosia cordifolia</i>	Sonoran Desert	C_3	-37.5	-115
<i>Ambrosia deltoidea</i>	Sonoran Desert	C_3	-31.8	-116
<i>Aristida ternipes*</i>	Sonoran Desert	C_4	-29.1	-158
<i>Brongniartia tenuifolia</i>	Thornscrub	C_3	no data	-124
<i>Bursera laxiflora</i>	Thornscrub	C_3	no data	-151
<i>Bursera microflora</i>	Thornscrub	C_3	no data	-132
<i>Cathestecum brevifolium*</i>	Sonoran Desert	C_4	-27.1	-164
<i>Dyschoriste hirsutissima</i>	Thornscrub	C_3	no data	-137
<i>Encelia farinosa</i>	Sonoran Desert	C_3	-30.9	-149
<i>Eupatorium sagittatum</i>	Sonoran Desert	C_3	no data	-142
<i>Chromolaena sagittata</i>	Thornscrub	C_3	no data	-145
<i>Forchhammeria watsonii</i>	Thornscrub	C_3	no data	-90
<i>Fouquieria macdougalii</i>	Thornscrub	C_3	no data	-143
<i>Guaiacum coulteri</i>	Thornscrub	C_3	no data	-113
<i>Haematoxylon brasiletto</i>	Thornscrub	C_3	-34.8	-126
<i>Henrya insularis</i>	Thornscrub	C_3	no data	-145
<i>Ipomoea arborescens</i>	Thornscrub	C_3	no data	-126
<i>Jacquinia macrocarpa</i>	Thornscrub	C_3	no data	-157
<i>Jatropha cartiophylla</i>	Sonoran Desert	C_3	-30.1	-179
<i>Larrea tridentata</i>	Sonoran Desert	C_3	-31.7	-116
<i>Melochia tomentosa</i>	Thornscrub	C_3	no data	-155
<i>Muhlenbergia porteri*</i>	Sonoran Desert	C_4	-26.5	-162
<i>Olneya tesota</i>	Sonoran Desert	C_3	-30.1	-111
<i>Parkinsonia microphylla</i>	Sonoran Desert	C_3	-31.9	-156
<i>Piscidia mollis</i>	Sonoran Desert	C_3	no data	-149
<i>Prosopis velutina</i>	Sonoran Desert	C_3	no data	-106
<i>Randia echinocarpa</i>	Sonoran Desert	C_3	no data	-119
<i>Simmondsia chinensis</i>	Sonoran Desert	C_3	-31.8	-134
<i>Solanum tridynamum</i>	Thornscrub	C_3	no data	-150
<i>Trixis californica</i>	Sonoran Desert	C_3	-37.2	-138
<i>Vachellia campechiana</i>	Thornscrub	C_3	no data	-119
<i>Vachellia constricta</i>	Thornscrub	C_3	-37.1	-105

Table S3. End-members of $\delta^{13}\text{C}$ and ε_{p-w} used for our calculation of leaf wax-inferred δD_p . $\delta^{13}\text{C}$ values have been corrected for the Suess effect. All carbon end-members come from modern plants at the Arizona-Sonora Desert Museum

Value	Mean	Standard Error	Sample Size
$\delta^{13}\text{C}_3$ (Eudicots)	-32.1	0.7	12
$\delta^{13}\text{C}_4$ (Graminoids)	-26.5	2.3	3
ε_{C4} (Eudicots)	-113	3	3
ε_{C3} (Graminoids)	-81	4	31

Table S4. Overview of iCAM5 simulations used in this study, along with the response they identify (see Text S1). Simulations include an idealized SST run following Fu et al. (2022), as well as six sensitivity experiments.

Experiment	Description	Response
Pliocene SSTs	SST pattern from (Fu et al., 2022)	Hydroclimate response to Pliocene SSTs
1°C Uniform	1°C warming + CESM1.2 coupled SSTs	Uniform warming with no pattern change
2°C Uniform	2°C warming + CESM1.2 coupled SSTs	Uniform warming with no pattern change
1x MHW	1x MHW pattern + CESM1.2 coupled SSTs	Amplified Subtropical warming relative to EEP
2x MHW	2x MHW pattern + CESM1.2 coupled SSTs	Amplified Subtropical warming relative to EEP
3x MHW	3x MHW pattern + CESM1.2 coupled SSTs	Amplified Subtropical warming relative to EEP
4x MHW	4x MHW pattern + CESM1.2 coupled SSTs	Amplified Subtropical warming relative to EEP

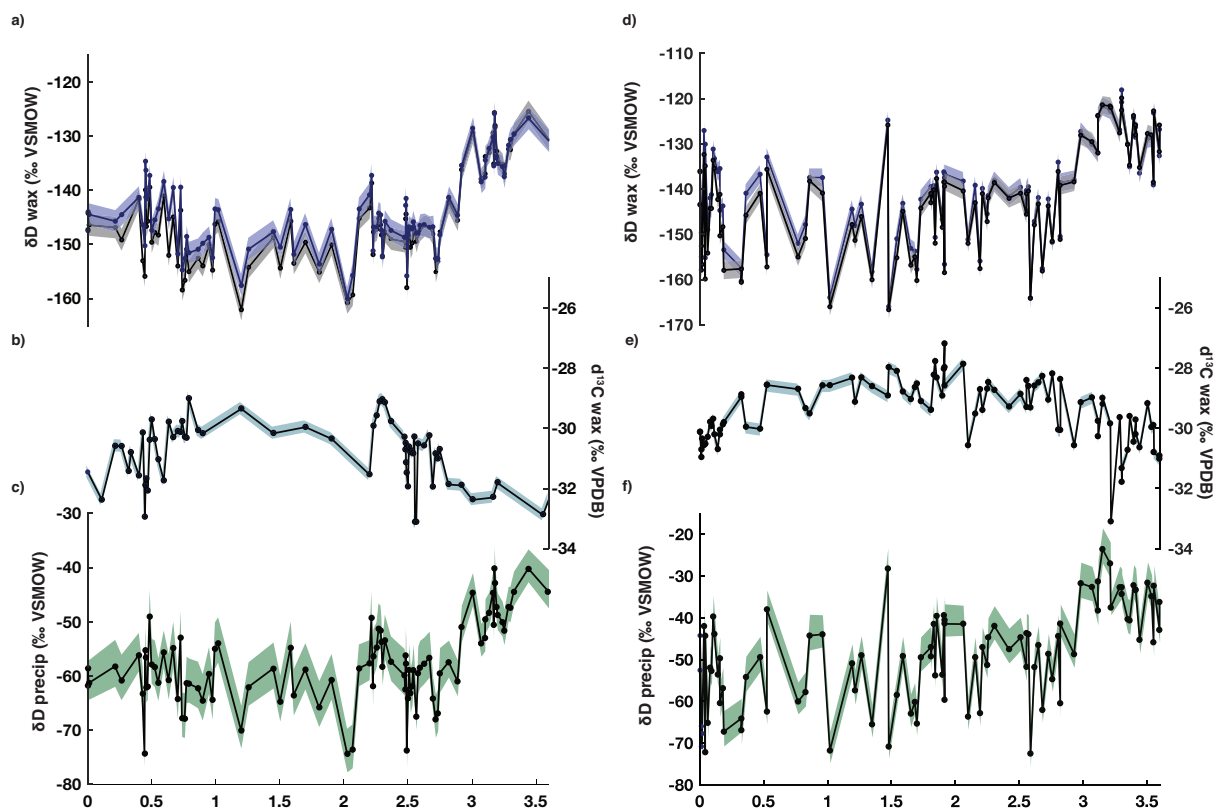


Figure S1. C_{30} alkanic acid δD , $\delta^{13}C$, and inferred δD_p from sites DSDP 475 (left) and ODP 1012 (right). All values are shown with 1σ uncertainties. a) and d) show δD of the C_{30} alkanic acid, with gray curve reflecting ice-volume corrected values. The effect of a million-year ice volume correction is extremely minor. b) and e) show carbon isotope data with 1σ analytical error. At site 475, carbon isotopes were analyzed at a lower resolution since for several depths sample material was consumed for hydrogen isotope analysis. c) and f) show inferred δD_p values for each site. Note the larger uncertainty that includes analytical uncertainty and uncertainty from the Bayesian mixing model.

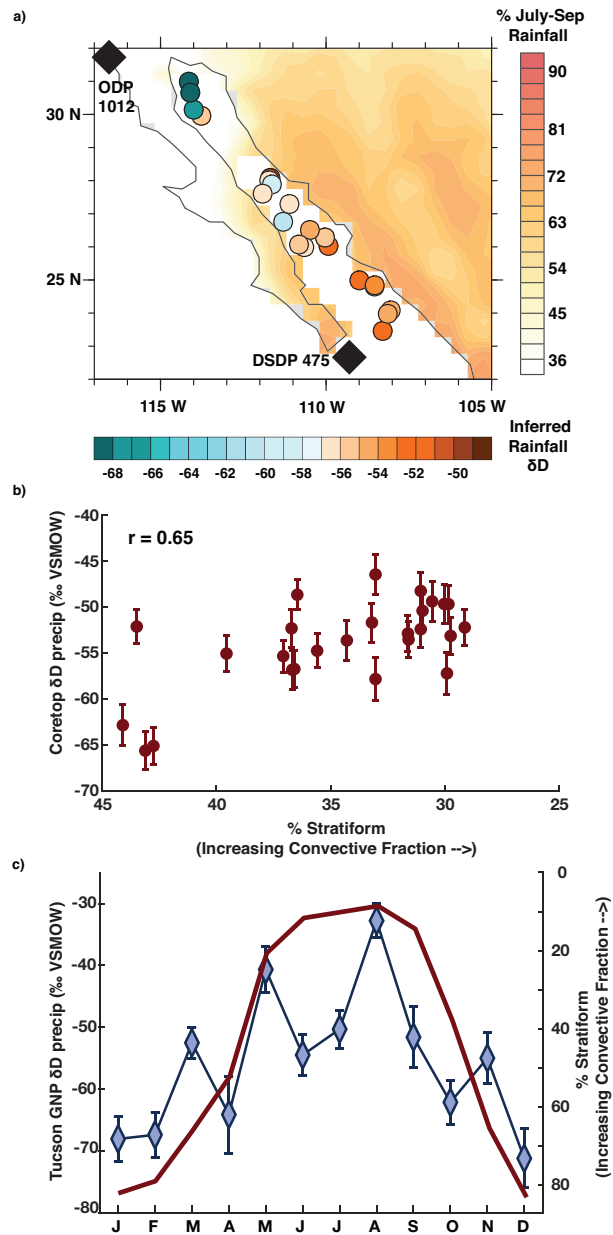


Figure S2. a) Coretop-inferred δD_p in the Gulf of California from Bhattacharya et al. (2018). Original data are replotted using updated $\delta^{13}C$ and ϵ_{p-w} corrections from Table S2. Background contours indicate the percentage of NAM contribution to annual rainfall. b) Coretop δD_p plotted against the percentage of rainfall on adjacent land regions that derives from stratiform rainfall (decreasing stratiform fraction indicates a greater share of convective precipitation). Stratiform fraction is used following the convention of Aggarwal et al. (2016). c) Seasonal cycle in Tucson GNIP station (Eastoe & Dettman, 2016) δD_p versus percent stratiform rainfall.

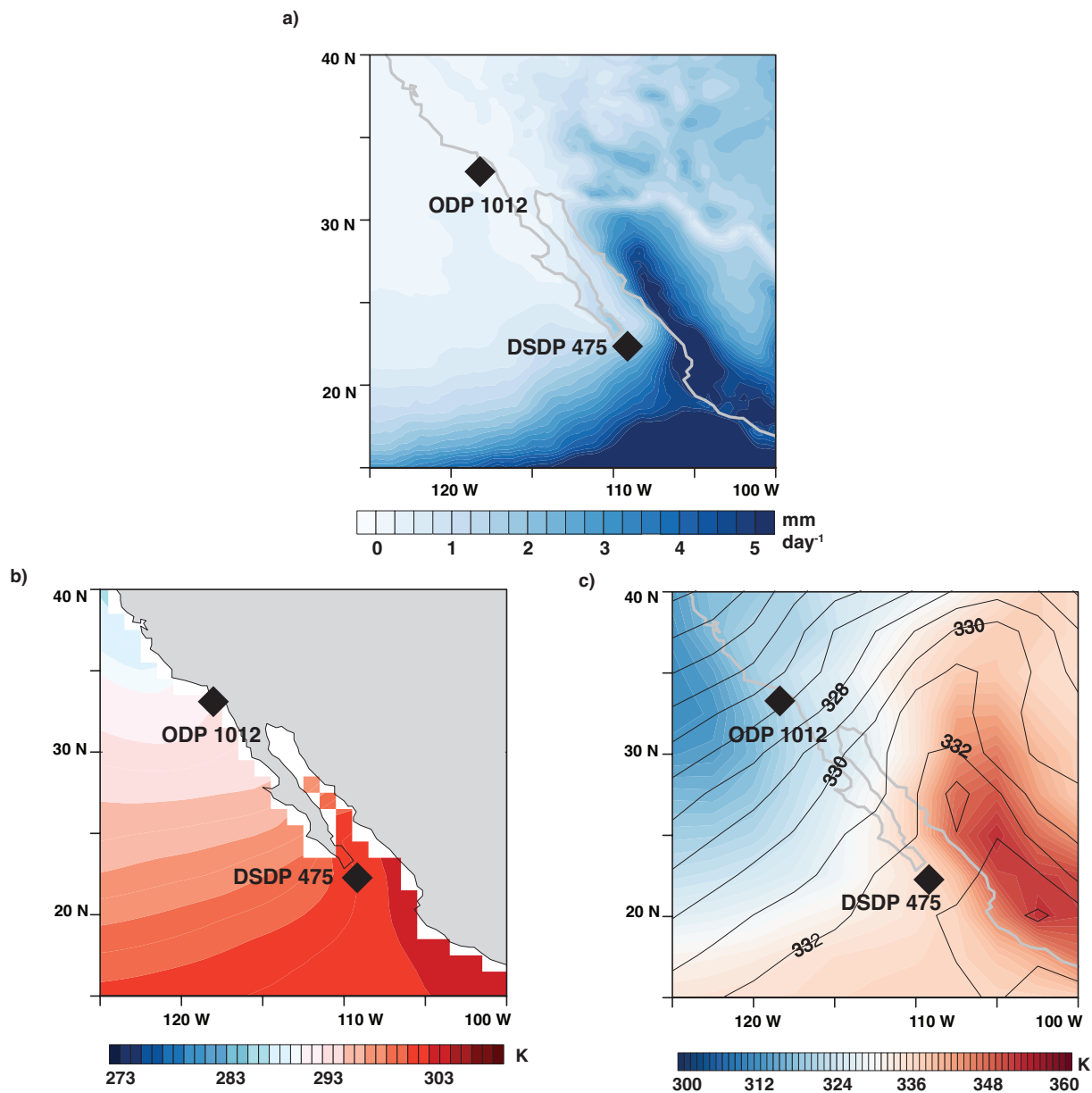


Figure S3. July-September climatology, calculated from 1950 - 2018, of a) rainfall in mm/day, b) sea surface temperatures, and c) equivalent potential temperature or θ_e (solid contours are mid-tropospheric or 400 mb θ_e , while colored contours are low-level (surface to 900 mb) average θ_e). The location of DSDP 475 and ODP 1012 is indicated on each plot.

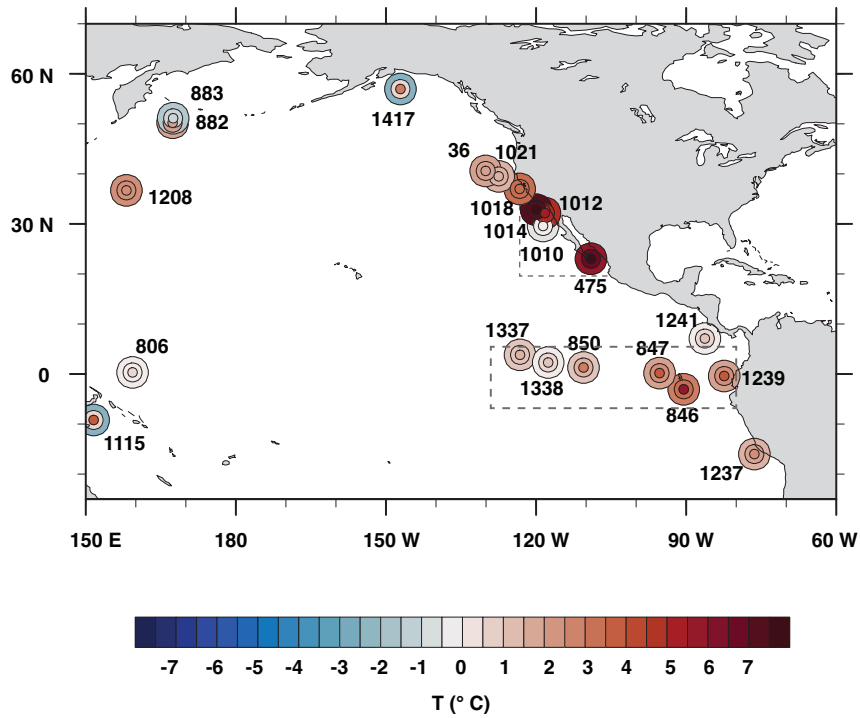


Figure S4. Mid-Pliocene (3.3 to 3.0 Ma) SST anomalies in alkenone-based temperature records across the north Pacific. Inner circle represents upper 95% confidence interval, middle circle is median value, while outer circle is the lower 95% confidence interval of ensemble estimates with analytical and calibration errors propagated through the time-series. Regions used to create averages of subtropical eastern Pacific (southern California Margin) and eastern equatorial Pacific SSTs are outlined in dashed rectangles.

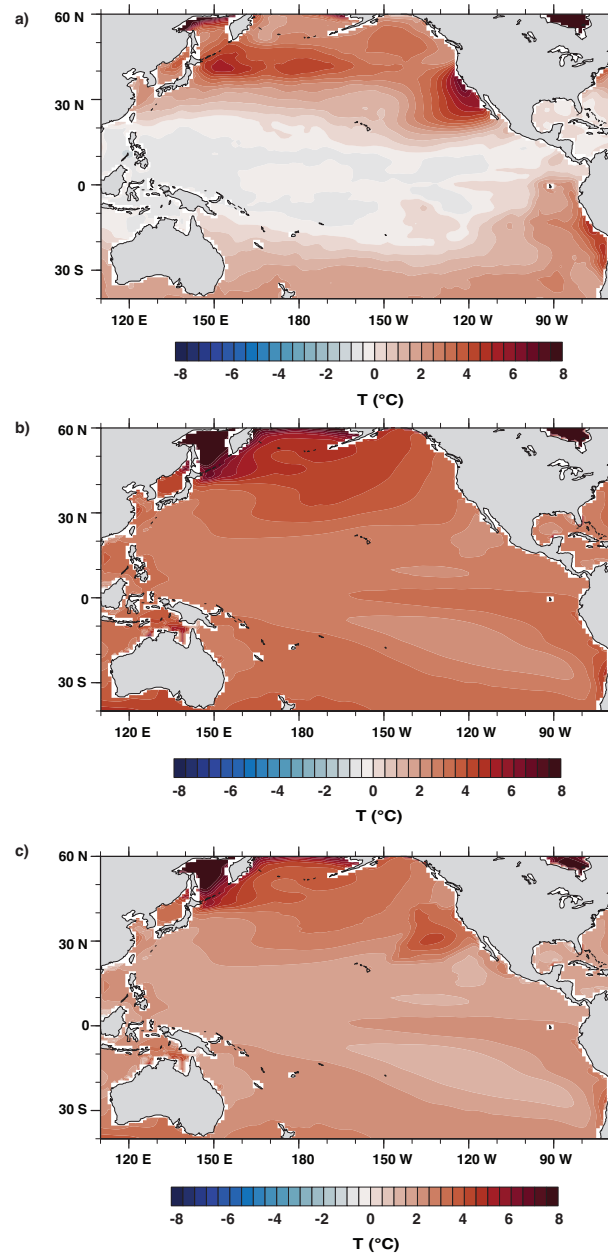


Figure S5. SST fields used for the iCAM5 simulations (see section 1 and Table S4. a) SSTs from Fu et al. (2022), which are also shown in Figure 2 in the main text. b) SSTs from a global 1 degree warming simulation. c) SST pattern with amplified coastal warming (taken from the 2014 marine heat wave). In Figure 3, we show results from iCAM5 simulations using 1x and 2x the warming pattern shown in panel b), as well as results from iCAM5 forced with 1x, 2x, 3x, and 4x the pattern in panel c).

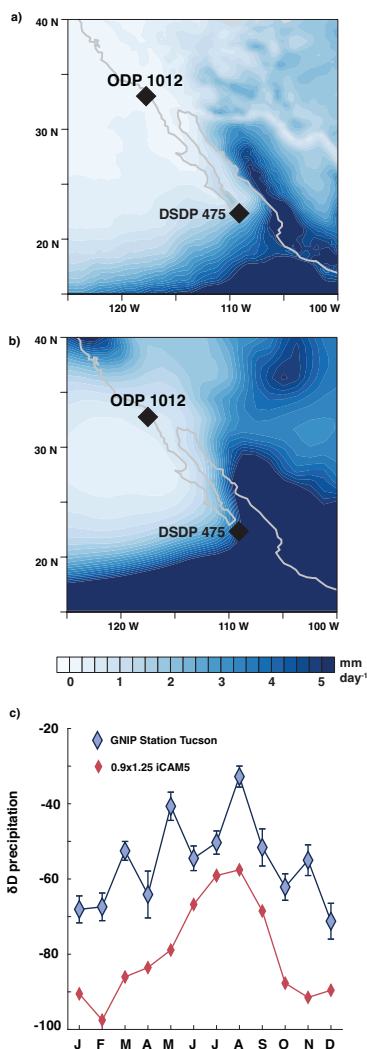


Figure S6. Observational vs. iCAM5 climatology for rainfall and the seasonal cycle of isotopes. a) GPCP July-September rainfall (Adler et al., 2018). b) Model climatology for the same interval. c) Climatology and standard error of measured precipitation δD from the Tucson GNIP station (Eastoe & Dettman, 2016) in dark blue compared to iCAM5's precipitation climatology for a region surrounding Tucson in red.